JOURNAL OF GUIDANCE, CONTROL, AND DYNAMICS
Vol. 41, No. 9, September 2018

Kinematic Steering Law for Conically Constrained Torque-Limited Spacecraft Attitude Control

Manuel Diaz Ramos* and Hanspeter Schaub†
University of Colorado, Boulder, Colorado 80309

DOI: 10.2514/1.G002873

A novel algorithm for attitude control of a spacecraft subjected to conically constrained inclusion and exclusion regions using a kinematic steering law and a rate-based attitude servo system is presented. The tracking errors are defined using switched modified Rodrigues parameters to yield, leveraging the nonuniqueness of the parametrization, a nonsingular description. Lyapunov theory and logarithmic barrier potential functions are used to derive a kinematic steering law suitable for both attitude regulation and tracking scenarios. Conditions for constraint enforcement under limited-control-torque capability are studied. Numerical examples of a regulation and a tracking problem are shown. A Monte Carlo simulation is performed to show constraint avoidance with a variety of worst-case initial conditions under bounded-torque control capabilities.

I. Introduction

UNCONSTRAINED autonomous attitude control has been extensively addressed in the literature. However, spacecraft reorientation may have several design-specific pointing restrictions. These attitude constraints can be in the form of undesirable pointing regions. An example is any spacecraft carrying heat- or light-sensitive instruments, such as telescopes or cameras, that cannot be exposed to direct sunlight. Bright celestial objects may thus impose constraints to a maneuver. On the other hand, pointing restrictions can also manifest themselves as inclusive heading regions. For example, a change in attitude could be performed while keeping certain instruments, for example, antennas or solar panels, pointing into a definite region in space. Ultimately, attitude constraints can be viewed as either exclusion or inclusion zones, usually defined by cones in space around either a forbidden or a mandatory nominal direction.

The existing techniques for studying the constrained attitude control problem may be classified into six different groups [1]. One approach uses geometric relations to precompute trajectories that avoid the constraint manifolds [2,3]. These techniques are relatively simple but do not scale well when the number of constraints grow [1]. A reactive geometric approach has been used in the SAMPEX mission to avoid its Heavy Ion Large Telescope (HILT) aligning with the velocity vector [4]. Another different geometric approach using an optimal boundary value problem and an iterative process has been recently developed [5]. Constraint monitor algorithms (CMT) use a predictor-corrector approach to change the trajectory in real time when approaching a constraint [1]. This method has been successfully tested in real missions, such as Cassini [6,7] and Deep-Space-1 [8]. Randomized algorithms use graphs and random search to go from an initial to a final attitude, avoiding all constraints [9]. The approach has mainly two drawbacks: convergence can be guaranteed only in a probabilistic sense and computational time grows dramatically with the size of the graph. The set of optimization techniques known as semi-definite programming (SDP) and quadratically constrained quadratic programming (QCQP) [10] can be used to compute an optimal control solution while avoiding all constraints [1,11,12]. A recently developed new framework divides the attitude space into discrete cells and uses searching algorithms like A^* to find an optimal solution to the constrained problem [13,14]. Finally, potential function-based algorithms use Lyapunov theory to design control laws that converge to the target while evading constraints. This approach has been proposed with singular Euler angles [15] and the unit-constrained quaternions [16,17] to solve the constrained regulation problem. In Ref. [18], another method using quaternions and a Hamiltonian formulation is proposed to handle one exclusion constraint using Lyapunov functions based on geometric considerations. However, it cannot be shown to converge, and may not even be feasible with several exclusion constraints.

In contrast to Euler angles and quaternions, the modified Rodrigues parameters (MRPs) constitute a singular, nonunique, and minimal attitude representation [19]. However, the nonuniqueness can be used to switch the parameters at the unit sphere in order to avoid their only singularity while naturally overcoming the unwinding [20] phenomenon, making a control scheme to always follow the shortest path [21].

Kinematic steering laws permit dividing the attitude and angular velocity control strategies into two completely separate loops, simplifying the synthesis of control laws [21,22]. Using this scheme, an angular velocity loop, usually known as servo subsystem, is controlled by a kinematic loop. The benefit of such attitude steering laws is that the angular velocity vector is treated as the control vector, and the rate response due to a tracking can be shaped in very general ways. In particular, the implementation discussed in Ref. [22] uses a smoothly saturated rate behavior. Thus, even with very large attitude tracking errors, the spacecraft closed-loop response reaches a predicable upper rate limit.

In spite of the fact that most mission requirements include constraints on slew maneuvers, the autonomous constrained attitude control literature is still sparse and many spacecraft perform constraint avoidance nonautonomously through open-loop attitude way point navigation solutions. Nonlinear control methods using Lyapunov theory have the advantage that they allow synthesizing relatively simple control laws, that is, control laws given by closed-form, usually analytic, functions. This fact makes these algorithms specially suitable for on-board implementation. Lyapunov theory has been applied before to the constrained attitude control regulation problem using Euler angles [15] and quaternions [16,17]. However, it has not yet been applied to solve the attitude tracking problem with constraints. Furthermore, the novel use of a kinematic steering law allows the use of rate saturating functions to control the maximum angular velocity. Additionally, no previous work has analyzed how constraint avoidance and reaction wheel (RW) torque saturation are related. Finally, the use of MRPs in this problem formulation is also novel in that the solution provides a minimal attitude parameterization that yields globally nonsingular behavior.

Received 28 February 2017; revision received 28 August 2017; accepted for publication 8 April 2018; published online 11 July 2018.

*Graduate Student, Department of Aerospace Engineering Sciences, 431 UCB, Colorado Center for Astrodynamics Research. Student Member AIAA.

†Alfred T. and Betty E. Look Professor of Engineering, Department of Aerospace Engineering Sciences, 431 UCB, Colorado Center for Astrodynamics Research. Associate Fellow AIAA.

In this work, a kinematic steering law using MRPs that permits autonomous attitude control and static constraint enforcement at the same time is proposed. Constraint geometry is discussed and Lyapunov direct method is used in order to synthesize the kinematic steering law. RWs are used as attitude actuators in the numerical simulation illustration. The problem of wheel torque saturation is addressed by investigating solutions to guarantee the constraint compliance even if the control torque actuation is limited.

The paper is organized as follows. After a brief introduction of the kinematics (MRPs), the kinetics (rigid body spacecraft with RW), and a review of the unconstrained steering law used, conic static constraints are presented, showing a novel description as a function of MRPs. The regulation and tracking problem with conic constraints are then developed with heuristic algorithms for asymptotic stability. The effect of RW torque saturation is studied. Finally, numerical simulation results are shown to demonstrate the autonomous constraint compliance.

II. Spacecraft Kinematic and Kinetic Equations of Motion

A. Modified Rodrigues Parameters

The MRPs are a minimal parametrization set of the rotation group SO(3). The MRP vector $\boldsymbol{\sigma}$ is defined in terms of the quaternion $\boldsymbol{\beta} = [\beta_0 \quad \beta_1 \quad \beta_2 \quad \beta_3]^T$ or the principal rotation vector representation $(\hat{\boldsymbol{e}}, \Phi)$ as [19,21,23,24]

$$\boldsymbol{\sigma} = \frac{1}{1+\beta_0}[\beta_1 \quad \beta_2 \quad \beta_3]^T = \tan\left(\frac{\Phi}{4}\right)\hat{\boldsymbol{e}} \tag{1}$$

where β_0 represents the scalar part of the quaternion. The representation is singular whenever $\beta_0 = -1$, where the rotation angle $\Phi = \pm 360°$.

The quaternion representation is not unique. In fact, because $\boldsymbol{\beta}$ and $-\boldsymbol{\beta}$ represent the same attitude, $\boldsymbol{\sigma}$ and $\boldsymbol{\sigma}^s$, known as the shadow set, also represent the same orientation, where [21,25]

$$\boldsymbol{\sigma}^s = -\frac{1}{1-\beta_0}[\beta_1 \quad \beta_2 \quad \beta_3]^T = -\frac{\boldsymbol{\sigma}}{\boldsymbol{\sigma}^T\boldsymbol{\sigma}} \tag{2}$$

Equation (1) shows that short rotations ($\Phi \le 180°$) have $\|\boldsymbol{\sigma}\|_2 \le 1$. Using this fact and the shadow set given in Eq. (2), the general approach is to switch between MRP representations at the unit sphere in order to avoid the singularity while always describing short rotations [21]. In other words, by leveraging the nonuniqueness of the parametrization, a minimal singularity-free attitude description can be obtained, using Eq. (2) to compute the MRPs whenever the attitude trajectory crosses the sphere given by $\|\boldsymbol{\sigma}\|_2 = 1$.

The rotation matrix $[C(\boldsymbol{\sigma})]$ that describes the orientation of a frame $\mathcal{P}$ relative to a frame $\mathcal{Q}$, also represented as $[PQ]$, can be computed from the MRP $\boldsymbol{\sigma}$ (or $\boldsymbol{\sigma}_{\mathcal{P}/\mathcal{Q}}$) as [21]

$$[C(\boldsymbol{\sigma})] = [I_{3\times3}] + \frac{8[\tilde{\boldsymbol{\sigma}}]^2 - 4(1-\boldsymbol{\sigma}^T\boldsymbol{\sigma})[\tilde{\boldsymbol{\sigma}}]}{(1+\boldsymbol{\sigma}^T\boldsymbol{\sigma})^2} \tag{3}$$

where $[\tilde{\boldsymbol{\sigma}}]$ is the associated skew-symmetric matrix [21]

$$[\tilde{\boldsymbol{\sigma}}] = \begin{bmatrix} 0 & -\sigma_3 & \sigma_2 \\ \sigma_3 & 0 & -\sigma_1 \\ -\sigma_2 & \sigma_1 & 0 \end{bmatrix} \tag{4}$$

The MRP kinematic differential equation is given by [21]

$$\dot{\boldsymbol{\sigma}} = \frac{1}{4}[(1-\boldsymbol{\sigma}^T\boldsymbol{\sigma})[I_{3\times3}] + 2[\tilde{\boldsymbol{\sigma}}] + \boldsymbol{\sigma}\boldsymbol{\sigma}^T]\boldsymbol{\omega} = \frac{1}{4}[B(\boldsymbol{\sigma})]\boldsymbol{\omega} \tag{5}$$

If $\boldsymbol{\sigma}$ represents the attitude of frame $\mathcal{P}$ relative to $\mathcal{Q}$ (noted as $\boldsymbol{\sigma}_{\mathcal{P}/\mathcal{Q}}$), then $\boldsymbol{\omega}$ is the angular velocity of frame $\mathcal{P}$ relative to $\mathcal{Q}$ written in $\mathcal{P}$-frame components (also noted as ${}^{\mathcal{P}}\boldsymbol{\omega}_{\mathcal{P}/\mathcal{Q}}$, where the left superscript notes the frame with respect to which the vector components are taken).

B. Rigid-Body Dynamics with Reaction Wheels

The rotational equations of motion of a rigid spacecraft with N_{RW} perfectly symmetric and balanced RWs are given by [21]

$$[I_{\mathrm{RW}}]\dot{\boldsymbol{\omega}} = -[\tilde{\boldsymbol{\omega}}]\Big([I_{\mathrm{RW}}]\boldsymbol{\omega} + [G_s]\boldsymbol{h}_s\Big) - [G_s]\boldsymbol{u}_s + \boldsymbol{L} \tag{6}$$

where

$$[I_{\mathrm{RW}}] = [I_s] + \sum_{i=1}^{N_{\mathrm{RW}}}\Big(J_{t_i}\hat{\boldsymbol{g}}_{t_i}\hat{\boldsymbol{g}}_{t_i}^T + J_{g_i}\hat{\boldsymbol{g}}_{g_i}\hat{\boldsymbol{g}}_{g_i}^T\Big) \tag{7}$$

$$[G_{\mathrm{s}}] = \begin{bmatrix} \hat{\boldsymbol{g}}_{s_1} & \cdots & \hat{\boldsymbol{g}}_{s_i} & \cdots & \hat{\boldsymbol{g}}_{s_{N_{\mathrm{RW}}}} \end{bmatrix} \tag{8}$$

$$\boldsymbol{h}_s = \Big[J_{s_1}(\hat{\boldsymbol{g}}_{s_1}^T\boldsymbol{\omega} + \Omega_1) \ \ldots \ J_{s_i}(\hat{\boldsymbol{g}}_{s_i}^T\boldsymbol{\omega} + \Omega_i) \ \ldots \ J_{s_N}(\hat{\boldsymbol{g}}_{s_{N_{\mathrm{RW}}}}^T\boldsymbol{\omega} + \Omega_{N_{\mathrm{RW}}})\Big]^T \tag{9}$$

$[I_{\mathrm{s}}]$ is the inertia tensor of the system with the wheels considered as point masses. A principal-axis frame $\mathcal{W}_i$:$\{\hat{\boldsymbol{g}}_{s_i}, \hat{\boldsymbol{g}}_{t_i}, \hat{\boldsymbol{g}}_{g_i}\}$ is attached to each RW, where $\hat{\boldsymbol{g}}_{s_i}$ is the direction of the spin axis. $[I_{w_i}] = \mathrm{diag}(J_{s_i}, J_{t_i}, J_{g_i})$ is the inertia matrix of each wheel written in the $\mathcal{W}$ frame relative to its center of mass. Ω_i is the angular velocity of the RW i relative to the spacecraft. The vector $\boldsymbol{u}_s$ contains the torques applied to each RW axis. The RW torque may saturate, with a maximum torque $u_{s_{\max}}$. $\boldsymbol{L}$ is the resultant external torque applied to the spacecraft.

The vector $\boldsymbol{\omega}$ is a shorthand notation for the angular velocity of the body frame relative to the inertial frame $\boldsymbol{\omega}_{\mathcal{B}/\mathcal{N}}$, where $\mathcal{B}$ is a body-fixed frame and $\mathcal{N}$ is an inertial frame. The over-dot symbol ($\dot{\bullet}$) represents an inertial derivative, and the prime symbol ($\bullet'$) represents a derivative relative to the rotating body frame. Although the equations of motion can be solved in any frame, it is assumed that every vector and tensor are written in the body-fixed frame $\mathcal{B}$.

III. Review of the Unconstrained MRP Steering Law

The goal of the unconstrained attitude control problem is to steer the body frame $\mathcal{B}$ to the reference frame $\mathcal{R}$. In other words, the relative attitude $\boldsymbol{\sigma}_{\mathcal{B}/\mathcal{R}}$ and angular velocity $\boldsymbol{\omega}_{\mathcal{B}/\mathcal{R}}$ are to be driven to zero. This problem can be solved using Lyapunov's direct method and two separate feedback loops for the attitude and the rate tracking [22], in a rather similar way as the backstepping control method [26,27] provides a cascaded control design that guarantees simultaneous stability of the kinematic and kinetic loops. However, the backstepping control technique imposes limitations on how the outer steering law is developed. Instead, this paper investigates a classic servo implementation where the outer loop and inner loop are individually stable, and the joint stability is ensured by letting the inner loop have a control bandwidth that is at least an order of magnitude faster. The benefit of this approach is that the outer kinematic steering loop can be more generally developed, as in this paper, whereas the limitation is that the rate tracking must be achieved with a tighter inner control loop.

A high-level block diagram is shown in Fig. 1. The block *dynamics* is given in Eq. (6). The block *kinematics* represents the kinematic differential equation given in Eq. (5). An inner *servo subsystem* loop controls angular velocity. An outer, slower loop, or *kinematic steering law*, controls attitude, taking angular velocity as a control force. Using two different loops for attitude and angular velocity has the following advantages. First, the kinematic model given by Eq. (5) is exact. Second, the synthesis of control laws is simplified. Third, as this paper demonstrates, the angular velocity servo loop does not need to be changed when static constraints are added.

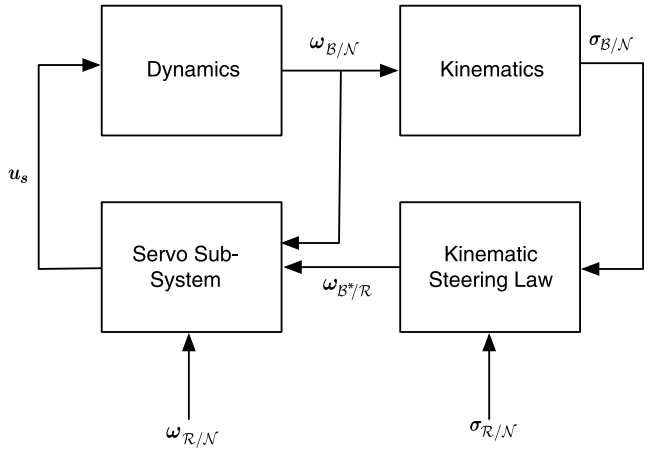

Fig. 1 Control system block diagram using a steering law.

Consider the following Lyapunov candidate function [21]

$$V(\boldsymbol{\sigma}_{\mathcal{B}/\mathcal{R}}) = 2\,\ell_n\left(1 + \boldsymbol{\sigma}_{\mathcal{B}/\mathcal{R}}^T\boldsymbol{\sigma}_{\mathcal{B}/\mathcal{R}}\right) \tag{10}$$

Using Eq. (5) it can be immediately shown that

$$\dot{V}(\boldsymbol{\sigma}_{\mathcal{B}/\mathcal{R}}) = \boldsymbol{\sigma}_{\mathcal{B}/\mathcal{R}}^T\boldsymbol{\omega}_{\mathcal{B}/\mathcal{R}} \tag{11}$$

Let $\mathcal{B}^*$ be the desired body orientation and $\boldsymbol{\omega}_{\mathcal{B}^*/\mathcal{R}}$ the desired angular velocity vector at which the spacecraft body should be rotating relative to the reference orientation. In other words, $\boldsymbol{\omega}_{\mathcal{B}^*/\mathcal{N}}$ is the set-point of the servo subsystem. Because the servo subsystem is supposed to be much faster than the outer loop, it is assumed, for the purpose of designing the outer loop, that $\mathcal{B}^* = \mathcal{B}$. In the following steering law, $\boldsymbol{\omega}_{\mathcal{B}^*/\mathcal{R}}$ is treated as a control variable, assuming that an inner rate servo loop exists that implements these speeds. The kinematic steering command is expressed as

$$\boldsymbol{\omega}_{\mathcal{B}^*/\mathcal{R}} = -\boldsymbol{f}(\boldsymbol{\sigma}_{\mathcal{B}/\mathcal{R}}) \tag{12}$$

where $\boldsymbol{f}(\boldsymbol{\sigma}_{\mathcal{B}/\mathcal{R}})$ is an odd function such that

$$\boldsymbol{\sigma}_{\mathcal{B}/\mathcal{R}}^T\boldsymbol{f}(\boldsymbol{\sigma}_{\mathcal{B}/\mathcal{R}}) > 0 \tag{13}$$

The Lyapunov rate will, thus, be negative definite:

$$\dot{V}(\boldsymbol{\sigma}_{\mathcal{B}/\mathcal{R}}) = -\boldsymbol{\sigma}_{\mathcal{B}/\mathcal{R}}^T\boldsymbol{f}(\boldsymbol{\sigma}_{\mathcal{B}/\mathcal{R}}) < 0 \quad \forall\ \boldsymbol{\sigma}_{\mathcal{B}/\mathcal{R}} \neq \boldsymbol{0} \tag{14}$$

In this paper, the smoothly saturated function given by [22]

$$f(x_i) = \frac{2\omega_{\max}}{\pi}\arctan\left(\frac{\pi}{2\omega_{\max}}(K_1 x_i + K_3 x_i^3)\right) \quad i = 1, 2, 3 \tag{15}$$

is used, where $\boldsymbol{f}(\boldsymbol{\sigma}_{\mathcal{B}/\mathcal{R}}) = [\,f(\sigma_1) \quad f(\sigma_2) \quad f(\sigma_3)\,]^T$.

A servo subsystem is used to produce the required torques to make the body rates track the desired body rates commanded by the steering law. Equivalently, the goal of the servo subsystem is to drive $\mathcal{B}$ to $\mathcal{B}^*$. The tracking error is defined as

$$\boldsymbol{\omega}_{\mathcal{B}/\mathcal{B}^*} = \boldsymbol{\omega}_{\mathcal{B}/\mathcal{N}} - \boldsymbol{\omega}_{\mathcal{B}^*/\mathcal{N}} = \boldsymbol{\omega}_{\mathcal{B}/\mathcal{N}} - \boldsymbol{\omega}_{\mathcal{B}^*/\mathcal{R}} - \boldsymbol{\omega}_{\mathcal{R}/\mathcal{N}} \tag{16}$$

where the fact that $\boldsymbol{\omega}_{\mathcal{B}^*/\mathcal{N}} = \boldsymbol{\omega}_{\mathcal{B}^*/\mathcal{R}} + \boldsymbol{\omega}_{\mathcal{R}/\mathcal{N}}$ has been used. $\boldsymbol{\omega}_{\mathcal{B}^*/\mathcal{R}}$ is the kinematic steering rate command and $\boldsymbol{\omega}_{\mathcal{R}/\mathcal{N}}$ is an input coming from the attitude navigation solution that generates a reference trajectory. To create a rate-servo that is robust to unmodeled torques [21], the integral term z is defined as

$$z = \int_{t_0}^{t} \boldsymbol{\omega}_{\mathcal{B}/\mathcal{B}^*}\,\mathrm{d}\tau \tag{17}$$

Consider the Lyapunov candidate function [22]

$$V_\omega(\boldsymbol{\omega}_{\mathcal{B}/\mathcal{B}^*}, z) = \frac{1}{2}\boldsymbol{\omega}_{\mathcal{B}/\mathcal{B}^*}^T[I_{\mathrm{RW}}]\boldsymbol{\omega}_{\mathcal{B}/\mathcal{B}^*} + \frac{1}{2}z^T[K_{\mathrm{I}}]z \tag{18}$$

where $[K_{\mathrm{I}}]$ is a positive definite matrix. Thus

$$\dot{V}_\omega(\boldsymbol{\omega}_{\mathcal{B}/\mathcal{B}^*}, z) = \boldsymbol{\omega}_{\mathcal{B}/\mathcal{B}^*}^T\left([I_{\mathrm{RW}}]\boldsymbol{\omega}'_{\mathcal{B}/\mathcal{B}^*} + [K_{\mathrm{I}}]z\right) \tag{19}$$

Using the identities $\boldsymbol{\omega}'_{\mathcal{B}/\mathcal{N}} = \dot{\boldsymbol{\omega}}_{\mathcal{B}/\mathcal{N}}$ and $\boldsymbol{\omega}'_{\mathcal{R}/\mathcal{N}} = \dot{\boldsymbol{\omega}}_{\mathcal{R}/\mathcal{N}} - \boldsymbol{\omega}_{\mathcal{B}/\mathcal{N}} \times \boldsymbol{\omega}_{\mathcal{R}/\mathcal{N}}$, and Eq. (16)

$$\boldsymbol{\omega}'_{\mathcal{B}/\mathcal{B}^*} = \dot{\boldsymbol{\omega}}_{\mathcal{B}/\mathcal{N}} - \boldsymbol{\omega}'_{\mathcal{B}^*/\mathcal{R}} - \dot{\boldsymbol{\omega}}_{\mathcal{R}/\mathcal{N}} + \boldsymbol{\omega}_{\mathcal{B}/\mathcal{N}} \times \boldsymbol{\omega}_{\mathcal{R}/\mathcal{N}} \tag{20}$$

Thus, using the spacecraft dynamics with RWs from Eq. (6)

$$\begin{aligned}\dot{V}_\omega(\boldsymbol{\omega}_{\mathcal{B}/\mathcal{B}^*}, z) = \boldsymbol{\omega}_{\mathcal{B}/\mathcal{B}^*}^T\Big[&-[\tilde{\boldsymbol{\omega}}_{\mathcal{B}/\mathcal{N}}]\left([I_{\mathrm{RW}}]\boldsymbol{\omega}_{\mathcal{B}/\mathcal{N}} + [G_s]\boldsymbol{h}_s\right) - [G_s]\boldsymbol{u}_s \\ &+ \boldsymbol{L} + [K_{\mathrm{I}}]z - [I_{\mathrm{RW}}]\left(\boldsymbol{\omega}'_{\mathcal{B}^*/\mathcal{R}} + \dot{\boldsymbol{\omega}}_{\mathcal{R}/\mathcal{N}} - \boldsymbol{\omega}_{\mathcal{B}/\mathcal{N}} \times \boldsymbol{\omega}_{\mathcal{R}/\mathcal{N}}\right)\Big]\end{aligned} \tag{21}$$

Forcing $\dot{V}_\omega = -\boldsymbol{\omega}_{\mathcal{B}/\mathcal{B}^*}^T[P]\boldsymbol{\omega}_{\mathcal{B}/\mathcal{B}^*}$, with $[P]$ being a positive definite matrix, it is possible to write

$$[G_s]\boldsymbol{u}_s = \boldsymbol{L}_r \tag{22}$$

where

$$\begin{aligned}\boldsymbol{L}_r = &[P]\boldsymbol{\omega}_{\mathcal{B}/\mathcal{B}^*} + [K_{\mathrm{I}}]z - [\tilde{\boldsymbol{\omega}}_{\mathcal{B}/\mathcal{N}}]\left([I_{\mathrm{RW}}]\boldsymbol{\omega}_{\mathcal{B}/\mathcal{N}} + [G_s]\boldsymbol{h}_s\right) \\ &- [I_{\mathrm{RW}}]\left(\boldsymbol{\omega}'_{\mathcal{B}^*/\mathcal{R}} + \dot{\boldsymbol{\omega}}_{\mathcal{R}/\mathcal{N}} - \boldsymbol{\omega}_{\mathcal{B}/\mathcal{N}} \times \boldsymbol{\omega}_{\mathcal{R}/\mathcal{N}}\right)\end{aligned} \tag{23}$$

In this paper, the RW torques are computed using the minimum norm inverse [21]

$$\boldsymbol{u}_s = [G_s]^T\left([G_s][G_s]^T\right)^{-1}\boldsymbol{L}_r \tag{24}$$

Equations (12) and (24) can be used to control a spacecraft's attitude using RWs without constraints. As with any kinematic steering law, the rate-servo subsystem needs to be faster than the outer loop to ensure both overall stability and that the assumption $\mathcal{B}^* = \mathcal{B}$ holds.

Because the algorithm requires the numerical computation of the integral $z = \int_{t_0}^{t}\boldsymbol{\omega}_{\mathcal{B}/\mathcal{B}^*}\,\mathrm{d}\tau$ and the body frame derivative $\boldsymbol{\omega}'_{\mathcal{B}^*/\mathcal{R}}$, a word is necessary on the numerical computation of these two magnitudes.

The integral term is numerically computed using the very simple trapezoidal rule [28], which consists on interpolating the integrand with a linear function.

The numerical derivative, however, is much more delicate. In fact, depending on the frequency of the servo subsystem loop and the frequency content of $\boldsymbol{\omega}_{\mathcal{B}^*/\mathcal{R}}$, significant noise can be injected into the control loop, requiring some kind of filtering on the torque command signals of the RW. The approach taken here is to compute the numerical derivative using the noise-prone backward difference [28]:

$$\boldsymbol{\omega}'_{\mathcal{B}^*/\mathcal{R}}(t_i) \approx f_{\mathrm{outer}}\left(\boldsymbol{\omega}_{\mathcal{B}^*/\mathcal{R}}(t_i) - \boldsymbol{\omega}_{\mathcal{B}^*/\mathcal{R}}(t_{i-1})\right) \tag{25}$$

where f_{outer} is the frequency of the outer loop.

However, the derivative is smoothed using a simple moving average [29]. The width of the window can be adjusted as a function of f_{outer}.

Because $\boldsymbol{\omega}'_{\mathcal{B}^*/\mathcal{R}}$ is a feed-forward term, its accuracy is not crucial. Indeed, it has been seen that, even in the case of overfiltering with a very wide window, the algorithm works well.

IV. Attitude Pointing Constraint Geometry Formulation

Orientation constraints can be classified as inclusion or exclusion constraints. In the first group, a given body-fixed direction has to be maintained pointing inside a definite region in space while a maneuver is being performed. On the other hand, exclusion constraints are classified into four different types [1]. In type I (static hard) constraints, there is "strict nonexposure constraints on the on-board sensitive instruments with respect to celestial objects" [1]. Conic constraints are a subtype, defined by a forbidden direction in space and a safety cone around it given by a constant angle. Type II (static soft constraints) is a relaxation of type I constraints in which violations of the forbidden zone are allowed, but for a limited amount of time. In other words, static soft constraints depend on attitude history. In type III (dynamic constraints), the forbidden region changes with time. A dynamic conic constraint is one in which the axis is not inertially fixed. Dynamic constraints can also be hard or soft. Finally, type IV (mixed constraints) includes any possible combination of the last three.

Henceforth, only conic constraints are considered. This particular static hard constraint is illustrated in Fig. 2, where an inertially fixed unit vector $\hat{\boldsymbol{n}}$ defines an exclusion or inclusion cone around it.

For an exclusion constraint, the goal is to slew a spacecraft avoiding a constant body-fixed unit vector $\hat{\boldsymbol{b}}$ entering the cone. The safety angle is given by $\theta_{\min}$, while θ is the instantaneous angle between both vectors. In a typical application $\hat{\boldsymbol{n}}$ can be a unit vector pointing toward the Sun (approximately inertially fixed) and $\hat{\boldsymbol{b}}$ is the boresight vector of a camera (body-fixed). Mathematically, the condition is described as [7]

$$\hat{\boldsymbol{n}} \cdot \hat{\boldsymbol{b}} = \cos(\theta) < \cos(\theta_{\min}) \tag{26}$$

Conic constraints are thus written introducing the rotation matrix $[BN]$ as

$$\begin{aligned} C_{[BN]}([BN]) &= \cos(\theta) - \cos(\theta_{\min}) = \hat{\boldsymbol{n}} \cdot \hat{\boldsymbol{b}} - \cos(\theta_{\min}) \\ &= {}^{\mathcal{N}}\hat{\boldsymbol{n}}^{T}[BN]^{T\,\mathcal{B}}\hat{\boldsymbol{b}} - \cos(\theta_{\min}) < 0 \end{aligned} \tag{27}$$

where the notation $C_{[BN]}$ indicates that the constraint is written as a function of the DCM.

Similarly, it might be desirable to maneuver while keeping a certain boresight vector $\hat{\boldsymbol{b}}$ inside a cone defined by $\hat{\boldsymbol{n}}$ and $\theta_{\min}$. For example, consider a maneuver that has to keep an antenna's main communication lobe inside a cone defined by a ground station, or maximize the area of the solar panels exposed to the Sun. The mathematical condition is

$$\hat{\boldsymbol{n}} \cdot \hat{\boldsymbol{b}} = \cos(\theta) > \cos(\theta_{\min}) \tag{28}$$

Thus, the constraint can be written as a function of the DCM as

$$\begin{aligned} C_{[BN]}([BN]) &= \cos(\theta) - \cos(\theta_{\min}) = \hat{\boldsymbol{n}} \cdot \hat{\boldsymbol{b}} - \cos(\theta_{\min}) \\ &= {}^{\mathcal{N}}\hat{\boldsymbol{n}}^{T}[BN]^{T\,\mathcal{B}}\hat{\boldsymbol{b}} - \cos(\theta_{\min}) > 0 \end{aligned} \tag{29}$$

It is important to note that exclusion and inclusion zones are defined using the same constraint formulation, namely, through a function $C_{[BN]}([BN])$. From the conic constraint definition, given the fact that $C_{[BN]}([BN])$ is the difference between two cosines, the following inequality constraint must be true:

$$-2 \le C_{[BN]}([BN]) \le 2 \tag{30}$$

An expression for $\dot{C}_{[BN]}([BN])$ is readily computed using the transport theorem [21] and the circular shift property of the triple product. If the derivatives are taken in the inertial frame under the hypothesis that $\hat{\boldsymbol{n}}$ is inertially constant and $\hat{\boldsymbol{b}}$ is body-fixed, then

$$\begin{aligned} \dot{C}_{[BN]}([BN]) &= \frac{{}^{\mathcal{N}}\mathrm{d}\hat{\boldsymbol{n}}}{\mathrm{d}t} \cdot \hat{\boldsymbol{b}} + \hat{\boldsymbol{n}} \cdot \frac{{}^{\mathcal{N}}\mathrm{d}\hat{\boldsymbol{b}}}{\mathrm{d}t} = \hat{\boldsymbol{n}} \cdot \left(\boldsymbol{\omega}_{\mathcal{B}/\mathcal{N}} \times \hat{\boldsymbol{b}}\right) \\ &= (\hat{\boldsymbol{b}} \times \hat{\boldsymbol{n}}) \cdot \boldsymbol{\omega}_{\mathcal{B}/\mathcal{N}} = \left(\left[{}^{\mathcal{B}}\tilde{\boldsymbol{b}}\right][BN]^{\mathcal{N}}\hat{\boldsymbol{n}}\right)^{T\,\mathcal{B}}\boldsymbol{\omega}_{\mathcal{B}/\mathcal{N}} \end{aligned} \tag{31}$$

Using Eq. (3) the constraint and constraint rate expressions are rewritten as

$$C_{[BN]}[BN(\boldsymbol{\sigma}_{\mathcal{B}/\mathcal{N}})] = C_{\sigma}(\boldsymbol{\sigma}_{\mathcal{B}/\mathcal{N}}) = {}^{\mathcal{N}}\hat{\boldsymbol{n}}^{T}[BN(\boldsymbol{\sigma}_{\mathcal{B}/\mathcal{N}})]^{T\,\mathcal{B}}\hat{\boldsymbol{b}} - \cos(\theta_{\min}) \tag{32}$$

$$\dot{C}_{[BN]}[BN(\boldsymbol{\sigma}_{\mathcal{B}/\mathcal{N}})] = \dot{C}_{\sigma}(\boldsymbol{\sigma}_{\mathcal{B}/\mathcal{N}}) = \left([{}^{\mathcal{B}}\tilde{\boldsymbol{b}}][BN(\boldsymbol{\sigma}_{\mathcal{B}/\mathcal{N}})]^{\mathcal{N}}\hat{\boldsymbol{n}}\right)^{T\,\mathcal{B}}\boldsymbol{\omega}_{\mathcal{B}/\mathcal{N}} \tag{33}$$

V. Autonomous Constrained Attitude Control

A. Constraint Overview

Let there be N_E exclusion zones defined by continuous functions C_i^E: SO(3) $\to \mathbb{R}$ and N_I inclusion zones defined by continous functions C_j^I: SO(3) $\to \mathbb{R}$, which can be the $C_{[BN]}$ or the C_{σ} described in the previous section. Let $\mathcal{D}$ be such that

$$\mathcal{D} = \left\{x \in \mathrm{SO}(3) / C_i^E(x) < 0 \wedge C_j^I(x) > 0\right\} \tag{34}$$

The goal is to drive $\boldsymbol{\sigma}_{\mathcal{B}/\mathcal{R}}$ and $\boldsymbol{\omega}_{\mathcal{B}/\mathcal{R}}$ to zero while maneuvering inside $\mathcal{D}$. The first necessary condition is that $[BN] \in \mathcal{D}$ for all possible time.

Barrier functions have been used to design control laws avoiding constraints [15,16,30]. In this paper, logarithm barrier functions [16,17,30] are used to design Lyapunov functions that converge to the reference while avoiding the static constraints.

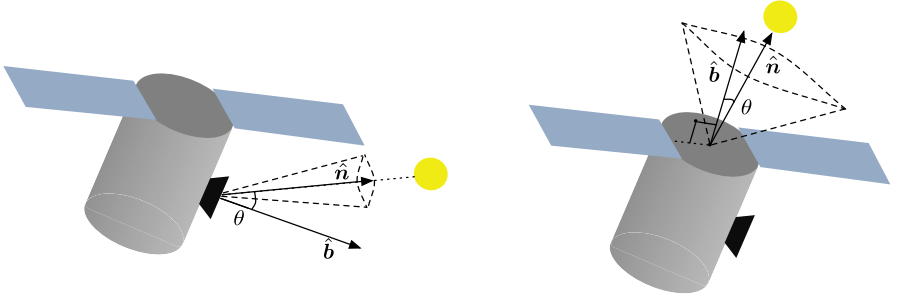

a) Conic exclusion constraint. The spacecraft has to slew keeping its sensitive optical instrument out of the sun-definecone

b) Conic inclusion constraint. The spacecraft has to slew keeping the solar panels pointing somewhere inside the sun-define cone

Fig. 2 Conic constraint geometry.

B. Constrained Regulation Problem

In the regulation problem, the goal is to steer $\boldsymbol{\sigma}_{\mathcal{B}/\mathcal{N}}$ and $\boldsymbol{\omega}_{\mathcal{B}/\mathcal{N}}$ to zero. The problem is split into two parts: a steering law and servo subsystem controlling angular velocity. Relative to the unconstrained laws, the latter remains the same. The steering law has to be changed.

Consider the following Lyapunov candidate function $V: \mathcal{D} \to \mathbb{R}^+$

$$V(\boldsymbol{\sigma}_{\mathcal{B}/\mathcal{N}}) = 2\,\ell_n(1+\boldsymbol{\sigma}_{\mathcal{B}/\mathcal{N}}^T\boldsymbol{\sigma}_{\mathcal{B}/\mathcal{N}})\left[-\frac{1}{N_E}\sum_{i=1}^{N_E}\ell_n\left(-\frac{C_i^E(\boldsymbol{\sigma}_{\mathcal{B}/\mathcal{N}})}{\alpha_i}\right) - \frac{1}{N_I}\sum_{j=1}^{N_I}\ell_n\left(\frac{C_j^I(\boldsymbol{\sigma}_{\mathcal{B}/\mathcal{N}})}{\beta_j}\right)\right] \tag{35}$$

The parameters $\alpha_i > 0$ and $\beta_j > 0$ may be chosen in several different ways with the only condition $-C_i^E(\boldsymbol{\sigma}_{\mathcal{B}/\mathcal{N}}) < \alpha_i$ and $C_j^I(\boldsymbol{\sigma}_{\mathcal{B}/\mathcal{N}}) < \beta_j$, $\forall \boldsymbol{\sigma}_{\mathcal{B}/\mathcal{N}} \in \mathcal{D}$. From Eq. (30), it can be seen that, for this condition to hold, $\alpha_i > 2$, $\beta_i > 2$. One valid choice is $\alpha_i = \beta_i = 2e$, such that the logarithm constraint terms are between 1 and $+\infty$. Another possibility for α_i is discussed later. These parameters also control the repelling force of the constraints. The larger α_i and β_i are, the steeper the barriers will be.

The function has the following characteristics:

1. $V(\boldsymbol{\sigma}_{\mathcal{B}/\mathcal{N}})$ is continuous if the MRP switching is performed at the unit sphere.
2. $V(\mathbf{0}) = 0$.
3. $V(\boldsymbol{\sigma}_{\mathcal{B}/\mathcal{N}}) > 0\ \forall \boldsymbol{\sigma}_{\mathcal{B}/\mathcal{N}} \in \{\mathcal{D} - \{\mathbf{0}\}\}$. Because $-C_i^E(\boldsymbol{\sigma}_{\mathcal{B}/\mathcal{N}}) < \alpha_i$, $C_j^I(\boldsymbol{\sigma}_{\mathcal{B}/\mathcal{N}}) < \beta_j$, and $-\ell_n(x)$ is a strictly decreasing function

$$\left[-\frac{1}{N_E}\sum_{i=1}^{N_E}\ell_n\left(-\frac{C_i^E(\boldsymbol{\sigma}_{\mathcal{B}/\mathcal{N}})}{\alpha_i}\right) - \frac{1}{N_I}\sum_{j=1}^{N_I}\ell_n\left(\frac{C_j^I(\boldsymbol{\sigma}_{\mathcal{B}/\mathcal{N}})}{\beta_j}\right)\right] > -N_E\,\ell_n(1) - N_I\,\ell_n(1) = 0 \tag{36}$$

Given the fact that $\ell_n(1+\boldsymbol{\sigma}_{\mathcal{B}/\mathcal{N}}^T\boldsymbol{\sigma}_{\mathcal{B}/\mathcal{N}}) > 0\ \forall\ \boldsymbol{\sigma}_{\mathcal{B}/\mathcal{N}} \in \{\mathcal{D} - \{\mathbf{0}\}\}$, thus $V(\boldsymbol{\sigma}_{\mathcal{B}/\mathcal{N}}) > 0\ \forall\ \boldsymbol{\sigma}_{\mathcal{B}/\mathcal{N}} \in \{\mathcal{D} - \{\mathbf{0}\}\}$.

4. $V(\boldsymbol{\sigma}_{\mathcal{B}/\mathcal{N}}) \to +\infty$ when $C_i^E(\boldsymbol{\sigma}_{\mathcal{B}/\mathcal{N}}) \to 0$ or $C_i^I(\boldsymbol{\sigma}_{\mathcal{B}/\mathcal{N}}) \to 0$.

Thus, $V(\boldsymbol{\sigma}_{\mathcal{B}/\mathcal{N}})$ is a proper Lyapunov function candidate. To derive a control law, the time derivative of V is computed:

$$\dot{V}(\boldsymbol{\sigma}_{\mathcal{B}/\mathcal{N}}) = \frac{4\boldsymbol{\sigma}_{\mathcal{B}/\mathcal{N}}^T\dot{\boldsymbol{\sigma}}_{\mathcal{B}/\mathcal{N}}}{(1+\boldsymbol{\sigma}_{\mathcal{B}/\mathcal{N}}^T\boldsymbol{\sigma}_{\mathcal{B}/\mathcal{N}})}\left[-\frac{1}{N_E}\sum_{i=1}^{N_E}\ell_n\left(-\frac{C_i^E(\boldsymbol{\sigma}_{\mathcal{B}/\mathcal{N}})}{\alpha_i}\right) - \frac{1}{N_I}\sum_{j=1}^{N_I}\ell_n\left(\frac{C_j^I(\boldsymbol{\sigma}_{\mathcal{B}/\mathcal{N}})}{\beta_j}\right)\right] + 2\,\ell_n(1+\boldsymbol{\sigma}_{\mathcal{B}/\mathcal{N}}^T\boldsymbol{\sigma}_{\mathcal{B}/\mathcal{N}}) \times\left[-\frac{1}{N_E}\sum_{i=1}^{N_E}\frac{\dot{C}_i^E(\boldsymbol{\sigma}_{\mathcal{B}/\mathcal{N}})}{C_i^E(\boldsymbol{\sigma}_{\mathcal{B}/\mathcal{N}})} - \frac{1}{N_I}\sum_{j=1}^{N_I}\frac{\dot{C}_j^I(\boldsymbol{\sigma}_{\mathcal{B}/\mathcal{N}})}{C_j^I(\boldsymbol{\sigma}_{\mathcal{B}/\mathcal{N}})}\right] \tag{37}$$

Using Eqs. (5) and (31)

$$\dot{V}(\boldsymbol{\sigma}_{\mathcal{B}/\mathcal{N}}) = \left(\boldsymbol{\sigma}_{\mathcal{B}/\mathcal{N}}^T\left[-\frac{1}{N_E}\sum_{i=1}^{N_E}\ell_n\left(-\frac{C_i^E(\boldsymbol{\sigma}_{\mathcal{B}/\mathcal{N}})}{\alpha_i}\right) - \frac{1}{N_I}\sum_{j=1}^{N_I}\ell_n\left(\frac{C_j^I(\boldsymbol{\sigma}_{\mathcal{B}/\mathcal{N}})}{\beta_j}\right)\right] + 2\,\ell_n(1+\boldsymbol{\sigma}_{\mathcal{B}/\mathcal{N}}^T\boldsymbol{\sigma}_{\mathcal{B}/\mathcal{N}}) \times\left[-\frac{1}{N_E}\sum_{i=1}^{N_E}\frac{([^{\mathcal{B}}\tilde{\boldsymbol{b}}][BN]^{\mathcal{N}}\hat{\boldsymbol{n}})^T}{C_j^E(\boldsymbol{\sigma}_{\mathcal{B}/\mathcal{N}})} - \frac{1}{N_I}\sum_{j=1}^{N_I}\frac{([^{\mathcal{B}}\tilde{\boldsymbol{b}}][BN]^{\mathcal{N}}\hat{\boldsymbol{n}})^T}{C_j^I(\boldsymbol{\sigma}_{\mathcal{B}/\mathcal{N}})}\right]\right)^{\mathcal{B}}\boldsymbol{\omega}_{\mathcal{B}/\mathcal{N}} \tag{38}$$

Letting $\boldsymbol{v}_R$ be

$$\boldsymbol{v}_R = \left(\boldsymbol{\sigma}_{\mathcal{B}/\mathcal{N}}\left[-\frac{1}{N_E}\sum_{i=1}^{N_E}\ell_n\left(-\frac{C_i^E(\boldsymbol{\sigma}_{\mathcal{B}/\mathcal{N}})}{\alpha_i}\right) - \frac{1}{N_I}\sum_{j=1}^{N_I}\ell_n\left(\frac{C_j^I(\boldsymbol{\sigma}_{\mathcal{B}/\mathcal{N}})}{\beta_j}\right)\right] + 2\,\ell_n(1+\boldsymbol{\sigma}_{\mathcal{B}/\mathcal{N}}^T\boldsymbol{\sigma}_{\mathcal{B}/\mathcal{N}})\left[-\frac{1}{N_E}\sum_{i=1}^{N_E}\frac{([^{\mathcal{B}}\tilde{\boldsymbol{b}}][BN]^{\mathcal{N}}\hat{\boldsymbol{n}})}{C_i^E(\boldsymbol{\sigma}_{\mathcal{B}/\mathcal{N}})} - \frac{1}{N_I}\sum_{j=1}^{N_I}\frac{([^{\mathcal{B}}\tilde{\boldsymbol{b}}][BN]^{\mathcal{N}}\hat{\boldsymbol{n}})}{C_j^I(\boldsymbol{\sigma}_{\mathcal{B}/\mathcal{N}})}\right]\right) \tag{39}$$

it is possible to write

$$\dot{V}(\boldsymbol{\sigma}_{\mathcal{B}/\mathcal{N}}) = \boldsymbol{v}_R^{T\mathcal{B}}\boldsymbol{\omega}_{\mathcal{B}/\mathcal{N}} \tag{40}$$

Whenever $\boldsymbol{\sigma}_{\mathcal{B}/\mathcal{N}} = \mathbf{0}$, $\boldsymbol{v}_R = \mathbf{0}$. However $\boldsymbol{v}_R$ can be zero for values other than $\boldsymbol{\sigma}_{\mathcal{B}/\mathcal{N}} = \mathbf{0}$. This situation is studied in a later section.

Choosing

$$^{\mathcal{B}}\boldsymbol{\omega}_{\mathcal{B}^*/\mathcal{N}} = -\boldsymbol{f}(\boldsymbol{v}_R) \tag{41}$$

where $\boldsymbol{f}$ is given by Eq. (15)

$$\dot{V}(\boldsymbol{\sigma}_{\mathcal{B}/\mathcal{N}}) = -\boldsymbol{v}_R^T\boldsymbol{f}(\boldsymbol{v}_R) \le 0 \tag{42}$$

According to Lyapunov's direct method [26], because $\dot{V}$ is negative semidefinite, the steering law given by Eq. (41) is stable, but not necessarily asymptotically stable ($\boldsymbol{v}_R = 0$ with $\boldsymbol{\sigma}_{\mathcal{B}/\mathcal{N}} \neq \mathbf{0}$).

C. Constrained Tracking Problem

In the tracking problem, the goal is to steer $\boldsymbol{\sigma}_{\mathcal{B}/\mathcal{R}}$ and $\boldsymbol{\omega}_{\mathcal{B}/\mathcal{R}}$ to zero. The problem is, again, split into two parts: a steering law and a servo subsystem controlling angular velocity. The servo is the same as used in the unconstrained problem.

Consider the following Lyapunov candidate function $V: \mathcal{D} \to \mathbb{R}^+$:

$$V(\boldsymbol{\sigma}_{\mathcal{B}/\mathcal{R}}) = 2\,\ell_n(1+\boldsymbol{\sigma}_{\mathcal{B}/\mathcal{R}}^T\boldsymbol{\sigma}_{\mathcal{B}/\mathcal{R}})\left[-\frac{1}{N_E}\sum_{i=1}^{N_E}\ell_n\left(-\frac{C_i^E(\boldsymbol{\sigma}_{\mathcal{B}/\mathcal{N}})}{\alpha_i}\right) - \frac{1}{N_I}\sum_{j=1}^{N_I}\ell_n\left(\frac{C_j^I(\boldsymbol{\sigma}_{\mathcal{B}/\mathcal{N}})}{\beta_j}\right)\right] \tag{43}$$

The parameters $\alpha_i > 0$ and $\beta_j > 0$ can be chosen as in the last section. V is a proper Lyapunov candidate function for the same reasons stated in the last section. Using Eqs. (5) and (31), and the fact that $\boldsymbol{\omega}_{\mathcal{B}/\mathcal{N}} = \boldsymbol{\omega}_{\mathcal{B}/\mathcal{R}} + \boldsymbol{\omega}_{\mathcal{R}/\mathcal{N}}$, its time derivative is given by

$$\dot{V}(\boldsymbol{\sigma}_{\mathcal{B}/\mathcal{R}}) = \left(\boldsymbol{\sigma}_{\mathcal{B}/\mathcal{R}}^T\left[\frac{1}{N_E}\sum_{i=1}^{N_E} - \ell_n\left(-\frac{C_i^E(\boldsymbol{\sigma}_{\mathcal{B}/\mathcal{N}})}{\alpha_i}\right) - \frac{1}{N_I}\sum_{j=1}^{N_I}\ell_n\left(\frac{C_j^I(\boldsymbol{\sigma}_{\mathcal{B}/\mathcal{N}})}{\beta_j}\right)\right] + 2\,\ell_n(1+\boldsymbol{\sigma}_{\mathcal{B}/\mathcal{R}}^T\boldsymbol{\sigma}_{\mathcal{B}/\mathcal{R}}) \times\left[-\frac{1}{N_E}\sum_{i=1}^{N_E}\frac{([^{\mathcal{B}}\tilde{\boldsymbol{b}}][BN]^{\mathcal{N}}\hat{\boldsymbol{n}})^T}{C_j^E(\boldsymbol{\sigma}_{\mathcal{B}/\mathcal{N}})} - \frac{1}{N_I}\sum_{j=1}^{N_I}\frac{([^{\mathcal{B}}\tilde{\boldsymbol{b}}][BN]^{\mathcal{N}}\hat{\boldsymbol{n}})^T}{C_j^I(\boldsymbol{\sigma}_{\mathcal{B}/\mathcal{N}})}\right]\right)^{\mathcal{B}}\boldsymbol{\omega}_{\mathcal{B}/\mathcal{R}} + 2\,\ell_n(1+\boldsymbol{\sigma}_{\mathcal{B}/\mathcal{R}}^T\boldsymbol{\sigma}_{\mathcal{B}/\mathcal{R}})\left[-\frac{1}{N_E}\sum_{i=1}^{N_E}\frac{([^{\mathcal{B}}\tilde{\boldsymbol{b}}][BN]^{\mathcal{N}}\hat{\boldsymbol{n}})^T}{C_j^E(\boldsymbol{\sigma}_{\mathcal{B}/\mathcal{N}})} - \frac{1}{N_I}\sum_{j=1}^{N_I}\frac{([^{\mathcal{B}}\tilde{\boldsymbol{b}}][BN]^{\mathcal{N}}\hat{\boldsymbol{n}})^T}{C_j^I(\boldsymbol{\sigma}_{\mathcal{B}/\mathcal{N}})}\right]^{\mathcal{B}}\boldsymbol{\omega}_{\mathcal{R}/\mathcal{N}} \tag{44}$$

Defining $\boldsymbol{v}_T$ and $\boldsymbol{u}_T$ such that

$$\boldsymbol{u}_T = 2\,\ell_n(1+\boldsymbol{\sigma}_{\mathcal{B}/\mathcal{R}}^T\boldsymbol{\sigma}_{\mathcal{B}/\mathcal{R}})\left[-\frac{1}{N_E}\sum_{i=1}^{N_E}\frac{([^{\mathcal{B}}\tilde{\boldsymbol{b}}][BN]^{\mathcal{N}}\hat{\boldsymbol{n}})}{C_j^E(\boldsymbol{\sigma}_{\mathcal{B}/\mathcal{N}})}\right.$$
$$\left.-\frac{1}{N_I}\sum_{j=1}^{N_I}\frac{([^{\mathcal{B}}\tilde{\boldsymbol{b}}][BN]^{\mathcal{N}}\hat{\boldsymbol{n}})}{C_j^I(\boldsymbol{\sigma}_{\mathcal{B}/\mathcal{N}})}\right] \tag{45}$$

$$\boldsymbol{v}_T = \boldsymbol{\sigma}_{\mathcal{B}/\mathcal{R}}\left[\frac{1}{N_E}\sum_{i=1}^{N_E}-\ell_n\left(-\frac{C_i^E(\boldsymbol{\sigma}_{\mathcal{B}/\mathcal{N}})}{\alpha_i}\right)-\frac{1}{N_I}\sum_{j=1}^{N_I}\ell_n\left(\frac{C_j^I(\boldsymbol{\sigma}_{\mathcal{B}/\mathcal{N}})}{\beta_j}\right)\right]$$
$$+\boldsymbol{u}_T \tag{46}$$

then

$$\dot{V}(\boldsymbol{\sigma}_{\mathcal{B}/\mathcal{R}}) = \boldsymbol{v}_T^{T\mathcal{B}}\boldsymbol{\omega}_{\mathcal{B}/\mathcal{R}} + \boldsymbol{u}_T^{T\mathcal{B}}\boldsymbol{\omega}_{\mathcal{R}/\mathcal{N}} \tag{47}$$

Choosing

$$^{\mathcal{B}}\boldsymbol{\omega}_{\mathcal{B}^*/\mathcal{R}} = -\boldsymbol{f}(\boldsymbol{v}_T) - \frac{\boldsymbol{v}_T\boldsymbol{u}_T^T}{\boldsymbol{v}_T^T\boldsymbol{v}_T}{}^{\mathcal{B}}\boldsymbol{\omega}_{\mathcal{R}/\mathcal{N}} \tag{48}$$

where $\boldsymbol{f}$ is given by Eq. (15)

$$\dot{V}(\boldsymbol{\sigma}_{\mathcal{B}/\mathcal{R}}) = -\boldsymbol{v}_T^T\boldsymbol{f}(\boldsymbol{v}_T) \le 0 \tag{49}$$

Because $\boldsymbol{\sigma}_{\mathcal{B}/\mathcal{R}} = \boldsymbol{0}$ implies $\boldsymbol{v}_T = \boldsymbol{u}_T = \boldsymbol{0}$, the second term in Eq. (48) contains a $0/0$ indetermination. However, $\ell_n(1+\boldsymbol{\sigma}_{\mathcal{B}/\mathcal{R}}^T\boldsymbol{\sigma}_{\mathcal{B}/\mathcal{R}}) \to \boldsymbol{\sigma}_{\mathcal{B}/\mathcal{R}}^T\boldsymbol{\sigma}_{\mathcal{B}/\mathcal{R}}$ when $\boldsymbol{\sigma}_{\mathcal{B}/\mathcal{R}} \to 0$. Thus it is possible to write

$$\boldsymbol{u}_T \underset{\boldsymbol{\sigma}_{\mathcal{B}/\mathcal{R}}\to 0}{\to} \boldsymbol{\sigma}_{\mathcal{B}/\mathcal{R}}^T\boldsymbol{\sigma}_{\mathcal{B}/\mathcal{R}}\boldsymbol{a} \tag{50}$$

$$\boldsymbol{v}_T \underset{\boldsymbol{\sigma}_{\mathcal{B}/\mathcal{R}}\to 0}{\to} \rho\boldsymbol{\sigma}_{\mathcal{B}/\mathcal{R}} + \boldsymbol{\sigma}_{\mathcal{B}/\mathcal{R}}^T\boldsymbol{\sigma}_{\mathcal{B}/\mathcal{R}}\boldsymbol{a} \tag{51}$$

The vector $\boldsymbol{a}$ and the scalar ρ do not depend on the attitude error. Therefore

$$\boldsymbol{v}_T^T\boldsymbol{v}_T \underset{\boldsymbol{\sigma}_{\mathcal{B}/\mathcal{R}}\to 0}{\to} \boldsymbol{\sigma}_{\mathcal{B}/\mathcal{R}}^T\boldsymbol{\sigma}_{\mathcal{B}/\mathcal{R}}\rho^2 + \left(\boldsymbol{\sigma}_{\mathcal{B}/\mathcal{R}}^T\boldsymbol{\sigma}_{\mathcal{B}/\mathcal{R}}\right)^2\boldsymbol{a}^T\boldsymbol{a} + 2\rho\boldsymbol{\sigma}_{\mathcal{B}/\mathcal{R}}^T\boldsymbol{\sigma}_{\mathcal{B}/\mathcal{R}}\boldsymbol{\sigma}_{\mathcal{B}/\mathcal{R}}^T\boldsymbol{a} \tag{52}$$

$$\boldsymbol{v}_T\boldsymbol{u}_T^{T\mathcal{B}}\boldsymbol{\omega}_{\mathcal{R}/\mathcal{N}} \underset{\boldsymbol{\sigma}_{\mathcal{B}/\mathcal{R}}\to 0}{\to} \rho\boldsymbol{\sigma}_{\mathcal{B}/\mathcal{R}}\boldsymbol{\sigma}_{\mathcal{B}/\mathcal{R}}^T\boldsymbol{\sigma}_{\mathcal{B}/\mathcal{R}}\boldsymbol{a}^{T\mathcal{B}}\boldsymbol{\omega}_{\mathcal{R}/\mathcal{N}}$$
$$+\left(\boldsymbol{\sigma}_{\mathcal{B}/\mathcal{R}}^T\boldsymbol{\sigma}_{\mathcal{B}/\mathcal{R}}\right)^2\boldsymbol{a}\boldsymbol{a}^{T\mathcal{B}}\boldsymbol{\omega}_{\mathcal{R}/\mathcal{N}} \tag{53}$$

When $\boldsymbol{\sigma}_{\mathcal{B}/\mathcal{R}} \to 0$, the expressions can be further approximated by dropping higher order terms

$$\boldsymbol{v}_T^T\boldsymbol{v}_T \underset{\boldsymbol{\sigma}_{\mathcal{B}/\mathcal{R}}\to 0}{\to} \boldsymbol{\sigma}_{\mathcal{B}/\mathcal{R}}^T\boldsymbol{\sigma}_{\mathcal{B}/\mathcal{R}}\rho^2 \tag{54}$$

$$\boldsymbol{v}_T\boldsymbol{u}_T^{T\mathcal{B}}\boldsymbol{\omega}_{\mathcal{R}/\mathcal{N}} \underset{\boldsymbol{\sigma}_{\mathcal{B}/\mathcal{R}}\to 0}{\to} \rho\boldsymbol{\sigma}_{\mathcal{B}/\mathcal{R}}\boldsymbol{\sigma}_{\mathcal{B}/\mathcal{R}}^T\boldsymbol{\sigma}_{\mathcal{B}/\mathcal{R}}\boldsymbol{a}^{T\mathcal{B}}\boldsymbol{\omega}_{\mathcal{R}/\mathcal{N}} \tag{55}$$

Hence

$$\frac{\boldsymbol{v}_T\boldsymbol{u}_T^T}{\boldsymbol{v}_T^T\boldsymbol{v}_T}{}^{\mathcal{B}}\boldsymbol{\omega}_{\mathcal{R}/\mathcal{N}} \underset{\boldsymbol{\sigma}_{\mathcal{B}/\mathcal{R}}\to 0}{\to} \frac{\rho\boldsymbol{\sigma}_{\mathcal{B}/\mathcal{R}}\boldsymbol{\sigma}_{\mathcal{B}/\mathcal{R}}^T\boldsymbol{\sigma}_{\mathcal{B}/\mathcal{R}}\boldsymbol{a}^{T\mathcal{B}}\boldsymbol{\omega}_{\mathcal{R}/\mathcal{N}}}{\boldsymbol{\sigma}_{\mathcal{B}/\mathcal{R}}^T\boldsymbol{\sigma}_{\mathcal{B}/\mathcal{R}}\rho^2}$$
$$= \frac{\boldsymbol{\sigma}_{\mathcal{B}/\mathcal{R}}\boldsymbol{a}^{T\mathcal{B}}\boldsymbol{\omega}_{\mathcal{R}/\mathcal{N}}}{\rho} \underset{\boldsymbol{\sigma}_{\mathcal{B}/\mathcal{R}}\to 0}{\to} 0 \tag{56}$$

This derivation solves the $0/0$ indetermination and shows that the second term can be modeled either by a linear function of the attitude error or by $\boldsymbol{0}$ when $\boldsymbol{\sigma}_{\mathcal{B}/\mathcal{R}}$ is small.

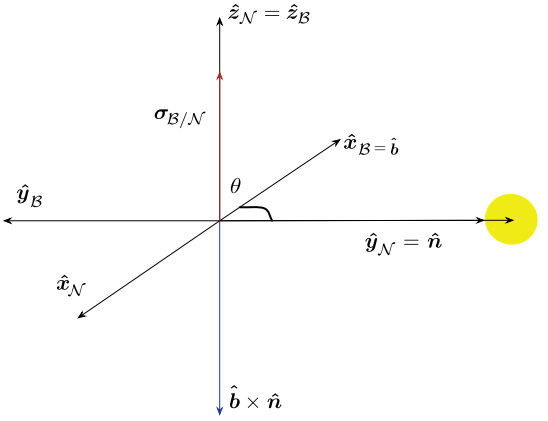

Fig. 3 With perfect symmetry $\boldsymbol{v}_R$ can be 0.

The vector $\boldsymbol{v}_T$ can also be zero for other values of $\boldsymbol{\sigma}_{\mathcal{B}/\mathcal{R}}$. This situation is studied in the following section.

VI. Convergence Analysis

It has been shown that the laws given by Eqs. (41) and (48) are Lyapunov stable but not necessarily asymptotically stable. Consider, for example, the special case in which $\boldsymbol{v}_T = \boldsymbol{0}$ and $\boldsymbol{\sigma}_{\mathcal{B}/\mathcal{R}} \neq \boldsymbol{0}$. Fortunately, it turns out that this occurs only with very specific symmetry conditions.

To understand the geometric conditions that lead to this situation, consider the following regulation problem ($\boldsymbol{\sigma}_{\mathcal{R}/\mathcal{N}} = \boldsymbol{0}$), depicted in Fig. 3. Let there only be one exclusion condition, given by $\hat{\boldsymbol{n}} = \hat{\boldsymbol{y}}_N$. The boresight vector is in the body $\hat{\boldsymbol{x}}$ direction: $\hat{\boldsymbol{b}} = \hat{\boldsymbol{x}}_B$. In this qualitative description, the angle $\theta_{\min}$ is not relevant. The initial attitude is a rotation of 180° about $\hat{\boldsymbol{z}}_N$. Thus $\boldsymbol{\sigma}_{\mathcal{B}/\mathcal{N}} = \tan(180°/4)\hat{\boldsymbol{z}}_N$.

The vector $\boldsymbol{v}_R$ will be

$$\boldsymbol{v}_R = -\boldsymbol{\sigma}_{\mathcal{B}/\mathcal{N}}\,\ell_n\left(-\frac{C_1^E(\boldsymbol{\sigma}_{\mathcal{B}/\mathcal{N}})}{\alpha_1}\right)$$
$$-2\,\ell_n(1+\boldsymbol{\sigma}_{\mathcal{B}/\mathcal{N}}^T\boldsymbol{\sigma}_{\mathcal{B}/\mathcal{N}})\frac{([^{\mathcal{B}}\tilde{\boldsymbol{b}}][BN]^{\mathcal{N}}\hat{\boldsymbol{n}})}{C_1^E(\boldsymbol{\sigma}_{\mathcal{B}/\mathcal{N}})} \tag{57}$$

A necessary (but not sufficient) condition for $\boldsymbol{v}_R$ to be zero with a nonzero $\boldsymbol{\sigma}_{\mathcal{B}/\mathcal{N}}$ is $\boldsymbol{\sigma}_{\mathcal{B}/\mathcal{N}}$ and $[^{\mathcal{B}}\tilde{\boldsymbol{b}}][BN]^{\mathcal{N}}\hat{\boldsymbol{n}}$ to be antiparallel. The latter is simply the vector $\hat{\boldsymbol{b}} \times \hat{\boldsymbol{n}}$ written in the body frame. In this particular case, that situation is possible because the attitude is a rotation about the $\hat{\boldsymbol{z}}_N$ axis and $\hat{\boldsymbol{b}} \times \hat{\boldsymbol{n}}$ is in the same direction. These saddle points can occur whenever the problem has one of these perfect symmetries. If the conic constraint is slightly tilted, the symmetry is broken, and no saddle point is reached for that attitude initial condition.

In practice, due to perturbations and numerical noise, saddle points occur very rarely. However, $\boldsymbol{v}_R$ (or $\boldsymbol{v}_T$) can become arbitrarily small.

A heuristic solution to avoid these saddle points is to detect whenever $\boldsymbol{v}_R$ (or $\boldsymbol{v}_T$) is small while $\boldsymbol{\sigma}_{\mathcal{B}/\mathcal{R}}$ is not and apply a very small push to the spacecraft in any direction orthogonal to $\boldsymbol{\sigma}_{\mathcal{B}/\mathcal{R}}$ in order to break the symmetry. The heuristic algorithm is shown as Algorithm 1. $\boldsymbol{\sigma}_{\mathcal{B}/\mathcal{R}}^{\perp}$ is any orthogonal vector to $\boldsymbol{\sigma}_{\mathcal{B}/\mathcal{R}}$. The scalar algorithm parameter γ is a small number to be chosen.

VII. Constraint Avoidance with Finite Control Torque

Even though the regulation control law given in Eq. (41) is bounded in angular velocity, it might require infinite angular

Algorithm 1: Saddle-point avoidance

1: **if** $\|\boldsymbol{v}_T\|_2$ (or $\|\boldsymbol{v}_R\|_2$) < 0.01 && $\|\boldsymbol{\sigma}_{\mathcal{B}/\mathcal{R}}\|_2 > 0.01$ **then**
2: $\quad\boldsymbol{v}_T$ (or $\boldsymbol{v}_R$) $= \gamma\boldsymbol{\sigma}_{\mathcal{B}/\mathcal{R}}^{\perp}$
3: **end if**

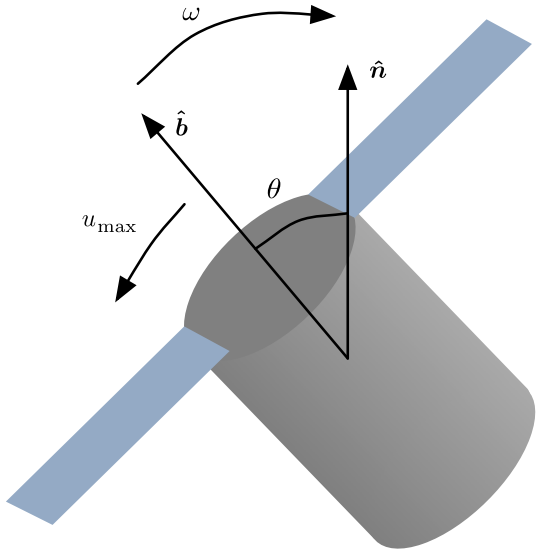

Fig. 4 Worst-case scenario. The spacecraft is rotating in a fixed plane at maximum angular velocity straight into a constraint. $u_{\max}$ is the maximum torque capacity in that direction.

acceleration when close to a constraint. To study how the control performs with limited torque capacity, Fig. 4 considers a very simple planar scenario. The boresight vector is rotating on a plane, moving forward toward a constraint cone. The inertia of the system about the fixed rotation axis is $I_{\max}$, the angular velocity is ω, and a constant available torque is given by $u_{\max}$. The angle at time t_0 is θ_0 and the initial angular velocity is ω_0. The problem can be stated as follows: with an inertia $I_{\max}$, constant control torque $u_{\max}$, and initial velocity $\omega_0 = \omega_{\max}$ given, what is the initial angle θ_0 to exactly stop the rotation at the safety cone given by the angle $\theta_{\min}$?

Because $\omega = -\dot{\theta}$, it is possible to write

$$\dot{\theta}_f = 0 = \frac{u_{\max}}{I_{\max}}(t_f - t_0) - \omega_{\max} \tag{58}$$

$$\theta_f = \theta_{\min} = \frac{1}{2}\frac{u_{\max}}{I_{\max}}(t_f - t_0)^2 - \omega_{\max}(t_f - t_0) + \theta_0 \tag{59}$$

Solving for $(t_f - t_0)$ in the first equation and replacing into the second

$$\theta_0 = \frac{1}{2}\frac{I_{\max}}{u_{\max}}\omega_{\max}^2 + \theta_{\min} \tag{60}$$

For a given spacecraft, $I_{\max}$ should be the maximum axis of inertia, $\omega_{\max}$ is the maximum velocity used in the steering law in Eq. (15) and $u_{\max}$ should be, at most, the maximum torque available in the poorest controllable direction. Given a maximum torque for each wheel $u_{s_{\max}}$, the minimum torque capacity for an RW array can be computed using torque envelopes. The algorithm for computing this minimum torque capacity is given in Ref. [31]. The maximum control torque magnitude that can be exerted by the RW array in the poorest controllable direction (u_{cap}) can be computed as follows:

$$u_{\text{cap}} = \min\left\{u_{i,j\,\min}; i, j = 1, \ldots, N_{\text{RW}}\right\} \tag{61}$$

$$u_{i,j\,\min} = u_{s_{\max}} \sum_{k=1,k\neq i,j}^{N_{\text{RW}}} |\hat{\boldsymbol{g}}_{s_k} \cdot \hat{\boldsymbol{p}}_{ij}| \tag{62}$$

$$\hat{\boldsymbol{p}}_{ij} = \frac{\hat{\boldsymbol{g}}_{s_i} \times \hat{\boldsymbol{g}}_{s_j}}{\|\hat{\boldsymbol{g}}_{s_i} \times \hat{\boldsymbol{g}}_{s_j}\|} \tag{63}$$

$u_{\max}$ used in Eq. (60) can be a fraction of the torque capacity in Eq. (61).

$$u_{\max} = \delta u_{\text{cap}}, \qquad 0 < \delta \leq 1 \tag{64}$$

Thus, for each exclusion constraint there is an angle $\theta_{\min}$ that defines the exclusion cone (inner cone) and an angle θ_0 that defines an outer cone. Using $\theta_{\min}$ in the constraint functions in Eqs. (41) and (48), the finite-torque control will not break through any exclusion constraint as long as the initial attitude is outside any outer cone and the angular velocity is not greater than $\omega_{\max}$.

VIII. Switching Between the Constrained and Unconstrained Laws

An additional use of the result of the last section enables switching between the constrained and unconstrained laws. When "far" from an exclusion constraint, it is possible to dismiss its inclusion in the control laws given by Eqs. (41) and (48). The angle θ_0 in Eq. (60) is used to evaluate this condition. The algorithm is shown as Algorithm 2. To avoid chattering, two different thresholds are defined using a hysteresis or Schmitt trigger [32] approach with a gap ψ.

This algorithm is repeated for every single exclusion constraint. Therefore, at a given instant of time, some constraints will be considered while others will not. That means eliminating those constraints that are not taken into account from Eqs. (39), (45), and (46).

To reduce (but not eliminate) the discontinuity while switching, the parameter α_i in Eq. (46) can be chosen such that $C_i^E(\boldsymbol{\sigma}_{\mathcal{B}/\mathcal{N}}) = \alpha_i$ when $\theta_i = \theta_{0i}$. From Eq. (29), $C_i^E(\boldsymbol{\sigma}_{\mathcal{B}/\mathcal{N}}) = \cos(\theta_i) - \cos(\theta_{\min i})$. Thus, picking α_i as

$$\alpha_i = \left|\cos\left(\frac{1}{2}\frac{I_{\max}}{u_{\max}}\omega_{\max}^2 + \theta_{\min i}\right) - \cos(\theta_{\min i})\right| e \tag{66}$$

would make the logarithm in Eq. (65) switch continuously when turning off the constraint algorithm.

IX. Numerical Simulation Results

To better show the behavior of the control algorithms introduced in this paper, three different simulations are performed. First, a regulation problem with spatial symmetry conditions aims at showing the saddle-point avoidance algorithm and how symmetry is related to the appearance of saddle points. A second numerical simulation illustrates the tracking problem with inclusion and exclusion constraints. Finally, a Monte Carlo simulation shows constraint avoidance under worst-case torque-limited conditions.

Parameters are indicated in Table 1. Four identical RWs in a pyramid configuration with an angle of 55° are used. The initial attitude is a simple rotation of −135° about the $\boldsymbol{x}$ axis. The initial angular velocity is full speed ($\omega_{\max} = 2°/\text{s}$) in the same direction. The four RWs are spinning at nominal speed (500 rpm).

Four exclusion constraints are used with an optical payload in the $\boldsymbol{y}$-body direction. One inclusion constraint (not used neither in the regulation example nor in the Monte Carlo run), with an antenna in the $\boldsymbol{x}$-body direction is also setup.

Algorithm 2: Constrained-Unconstrained control switching

1: Compute $[BN]$ from $\boldsymbol{\sigma}_{\mathcal{B}/\mathcal{N}}$ using Eq. (3)
2: Compute $\theta_i = \arccos({}^{\mathcal{N}}\hat{\boldsymbol{n}}_i^T [BN]^T {}^{\mathcal{B}}\hat{\boldsymbol{b}}_i)$
3: **if** $\theta_i < \theta_{0i} = \frac{1}{2}\frac{I_{\max}}{u_{\max}}\omega_{\max}^2 + \theta_{\min i}$ **then**
4: Use constrained control given in Eq. (48)
5: **else if** $\theta_i > \theta_{0i} + \psi$ **then**
6:
$$-\ell_n\left(-\frac{C_i^E(\boldsymbol{\sigma}_{\mathcal{B}/\mathcal{N}})}{\alpha_i}\right) \to 1 \qquad \frac{([{}^{\mathcal{B}}\tilde{\boldsymbol{b}}][BN]^{\mathcal{N}}\hat{\boldsymbol{n}})}{C_j^E(\boldsymbol{\sigma}_{\mathcal{B}/\mathcal{N}})} \to 0 \tag{65}$$
7: **end if**

Table 1 Simulation parameters

Description	Variable	Value
Spacecraft	$[I_S]$ [kg · m^2]	diag([4.415 4.415 3.83])
RW	$[I_w]$ [kg · m^2]	diag([0.03 0.001 0.001])
	$[G_s]$	$\begin{bmatrix} 0.819 & 0 & -0.819 & 0 \\ 0 & 0.819 & 0 & -0.819 \\ 0.5736 & 0.5736 & 0.5736 & 0.5736 \end{bmatrix}$
	$u_{s_{\max}}$	15 mN · m
Initial conditions	$\boldsymbol{\sigma}_{\mathcal{B}/\mathcal{N}_0}, \boldsymbol{\omega}_{\mathcal{B}/\mathcal{N}_0}$	$[-0.67 \quad 0 \quad 0]^T, [\omega_{\max} \quad 0 \quad 0]^T$
	$[\Omega_1 \quad \Omega_2 \quad \Omega_3 \quad \Omega_4]_0^T$	$[500 \quad -500 \quad 500 \quad -500]^T$ rpm
Control constants	$[P]$	$10[I_{3\times3}]$
	$[K_I]$	$0.01[I_{3\times3}]$
	K_1, K_3	0.1
Exclusion constraints	${}^{\mathcal{N}}\hat{\boldsymbol{n}}_1, {}^{\mathcal{B}}\hat{\boldsymbol{b}}_1, \theta_{\min 1}$	$[0 \quad -0.34 \quad -0.96]^T, [0 \quad 1 \quad 0]^T, 10^\circ$
	${}^{\mathcal{N}}\hat{\boldsymbol{n}}_2, {}^{\mathcal{B}}\hat{\boldsymbol{b}}_2, \theta_{\min 2}$	$[0 \quad -1 \quad 0]^T, [0 \quad 1 \quad 0]^T, 30^\circ$
	${}^{\mathcal{N}}\hat{\boldsymbol{n}}_3, {}^{\mathcal{B}}\hat{\boldsymbol{b}}_3, \theta_{\min 3}$	$[1 \quad 1 \quad 0]^T, [0 \quad 1 \quad 0]^T, 20^\circ$
	${}^{\mathcal{N}}\hat{\boldsymbol{n}}_4, {}^{\mathcal{B}}\hat{\boldsymbol{b}}_4, \theta_{\min 4}$	$[-1 \quad 1 \quad 0]^T, [0 \quad 1 \quad 0]^T, 20^\circ$
Inclusion constraints	${}^{\mathcal{N}}\hat{\boldsymbol{n}}_5, {}^{\mathcal{B}}\hat{\boldsymbol{b}}_5, \theta_{\min 5}$	$[1 \quad 0 \quad 0]^T, [1 \quad 0 \quad 0]^T, 60^\circ$

The servo subsystem given in Eq. (24) requires the computation of the body-frame derivative $\boldsymbol{\omega}'_{\mathcal{B}^*/\mathcal{R}}$. This derivative is numerically computed using backward difference [28] and a 0.5-s-window moving average in order to smooth the signal and avoid unnecessary noise

A. Regulation Problem

In this subsection, a regulation problem is simulated, with spatial symmetry relative to the initial conditions. The symmetric condition is achieved with four exclusion and no inclusion constraints. Because the problem is completely symmetric relative to the initial conditions, a saddle point is reached and Algorithm 1 is used with $\gamma = 0.01$ and $\boldsymbol{\sigma}^{\perp}_{\mathcal{B}/\mathcal{N}} = [-\sigma_3 \quad 0 \quad \sigma_1]$ if $\sigma_1 \neq 0$ or $\sigma_3 \neq 0$ and $\boldsymbol{\sigma}^{\perp}_{\mathcal{B}/\mathcal{N}} = [\sigma_2 \quad 0 \quad 0]$ in other case. Algorithm 2 is not used in order to show how the constrained control works on its own. $\alpha_i = \beta_i = 2e$ are used.

Figure 5 shows the results. As can be seen in Fig. 5b, the steering law generates a command of almost full speed in the opposite direction ($\omega_{1d}, \omega_{2d}, \omega_{3d}$ indicate the steering law commands) in order to brake the spacecraft. This angular velocity damping is associated to the existence of a saddle point. The situation is depicted in the cylindrical projection [16] in Fig. 5c. In this figure, the tip of the boresight vector in inertial space and the exclusion constraints (blobs) are projected into a right ascension-declination 2-D space. The dotted line indicates the path the unconstrained law would follow. The initial condition is such that the boresight vector is rotating straight into the near-south-pole constraint. The controller stops the rotation, reaches a saddle point, and, after using Algorithm 1 to getting out of it, rotates the spacecraft smoothly to the target.

For comparison, in Fig. 5d the fourth constraint is removed and the symmetry is broken. Thus, no saddle point is reached and the control is smoother. Furthermore, the spacecraft's angular velocity is not damped anymore because the symmetry is broken and the control is actually applying a torque with a large component perpendicular to the angular velocity. The vector $\boldsymbol{v}_R$ is never zero except when $\boldsymbol{\sigma}_{\mathcal{B}/\mathcal{N}} = \boldsymbol{0}$.

Finally, Fig. 5e shows the vector's norm $\|\boldsymbol{v}_R\|_2$ for the symmetric case depicted in Fig. 5c. As can be seen, a saddle point is reached when $\boldsymbol{v}_R \approx \boldsymbol{0}$. Fig. 5f, on the other side, shows the vector's norm $\|\boldsymbol{v}_R\|_2$ for the asymmetric case depicted in Fig. 5d. No saddle point is ever reached in this case.

B. Tracking Problem

In this example, the four exclusion and one inclusion constraints given in Table 1 are used. Algorithm 2 is used for switching between the constrained and unconstrained laws using a gap of $\psi = 5^\circ$. In Eq. (60), $u_{\max}$ is chosen to be 40% of the minimum torque capacity computed with Eq. (61). With this parameters, the angular difference between the inner and the outer cone is about 15°. α_i is picked according to Eq. (66) and $\beta_i = 2e$.

The reference frame $\mathcal{R}$ is constructed as follows. In a circular orbit around a perfectly spherical Earth, the direction $\hat{\boldsymbol{r}}_1$ is the nadir direction. $\hat{\boldsymbol{r}}_3$ is the angular momentum direction, normal to the orbit, and $\hat{\boldsymbol{r}}_2 = \hat{\boldsymbol{r}}_3 \times \hat{\boldsymbol{r}}_1$. Thus, $[RN] = [{}^{\mathcal{N}}\hat{\boldsymbol{r}}_1 \quad {}^{\mathcal{N}}\hat{\boldsymbol{r}}_2 \quad {}^{\mathcal{N}}\hat{\boldsymbol{r}}_3]^T$. The orbital parameters are shown in Table 2.

The results can be seen in Fig. 6. The cylindrical projections of the exclusion and inclusion zones in Figs. 6c and 6d show that the reference is tracked without violating any constraint.

The effect of using Algorithm 2 is shown in Fig. 7, where the four exclusion constraint angles, θ_1, θ_2, θ_3, θ_4, and the constraint minimum ($\theta_{\min}$) and threshold (θ_0) angles are plotted. The third and fourth exclusion constraints in Table 1 are so far from the trajectory that are not even considered by the control algorithm. The algorithm switches on and off constraints 1 and 2 using the threshold given in Eq. (60) and the hysteresis gap given by $\psi = 5^\circ$. After approximately 70 s, no constraint is used anymore and the purely unconstrained law is used instead.

C. Monte Carlo Simulation

A 50-run Monte Carlo simulation is shown in Fig. 8. A regulation problem is simulated 50 times for different initial conditions. The goal of the simulation is to statistically test the condition given by Eq. (60). To that end, different initial attitudes are generated such that the boresight vector of the camera is always rotating straight into the first exclusion constraint (see Table 1) at maximum angular velocity.

The first two exclusion zones in Table 1 are used. The initial attitude is random. The boresight vector of a camera is also randomly picked at some point on the outer cone of the first exclusion zone, computed using Eq. (60). The initial angular velocity is then calculated such that the boresight vector is rotating straight into the constraint with magnitude $\omega_{\max}$.

In the cylindrical projection in Fig. 8d, every single trajectory starts at the outer cone of the first exclusion constrained defined by the angle θ_0 in Eq. (60). The outer cone in Fig. 8d is represented by a lighter blob around the exclusion zone numbered as 1. This is shown in Fig. 8c, where the angle θ_1 at the start of every run corresponds to θ_0. As can be seen, the constraints are avoided with bounded angular velocity and limited torque (the maximum torque of each RW is 15 mN · m, see Fig. 8b), as long as the initial attitude is outside the outer cone. In Fig. 8c, the angle θ_1 is never below $\theta_{\min}$. This is a key result, because it shows that it is possible to avoid piercing an exclusion conic constraint, even with limited torque, if the initial

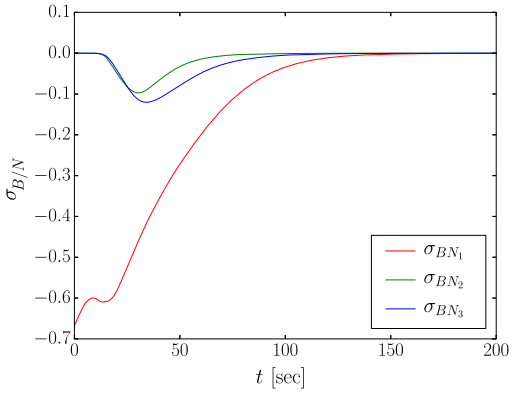

a) Attitude $\sigma_{B/N}$

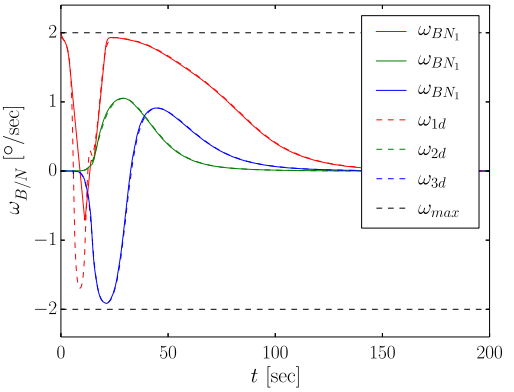

b) Angular velocity $\omega_{B/N}$

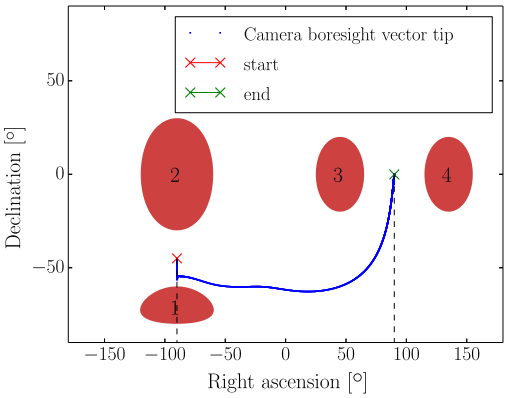

c) Cylindrical projection of the 3-D unit ball with symmetric conditions

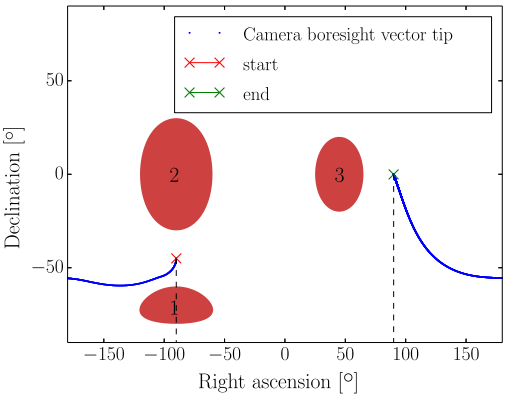

d) Cylindrical projection of the 3-D unit ball with asymmetric conditions

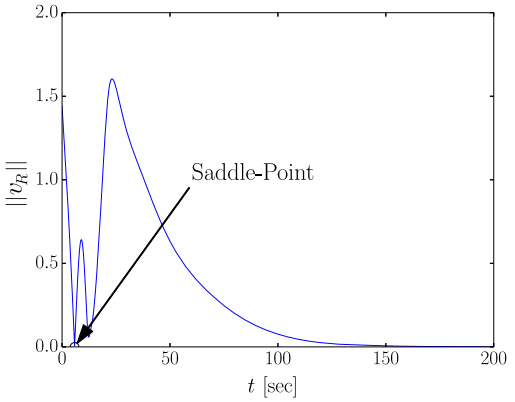

e) Norm $\|v_R\|_2$ with symmetric conditions

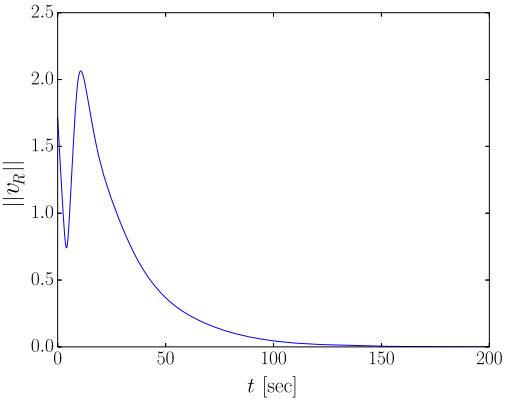

f) Norm $\|v_R\|_2$ with asymmetric conditions

Fig. 5 Regulation control performance illustration.

condition is outside an outer cone. The minimum angle defining this outer cone is related to the torque capacity of the RW configuration.

It can be seen in Fig. 8a that the transient closed-loop rates may temporarily exceed the maximum rate $\omega_{\max}$ (this is seen as a small peak in one run). Because a worst-case scenario with maximum rates is shown, this occurs very rarely and only for very small periods, and for small amounts. Moreover, it can be eliminated by tuning the control constants.

Table 2 Reference frame parameters

Description	Value
Earth's radius	6378.0 km
Earth's gravitational parameter	398600.0 km/s^2
Right ascension of ascending node	0°
Inclination	−90°
Orbit altitude	400 km
Initial argument of latitude	180°

X. Future Work

There are several questions that can be addressed in future work. First, the algorithm for escaping from saddle points has been explained heuristically, but not mathematically. Second, the algorithm switching between constrained and unconstrained laws still present some discontinuities. Future work might address further smoothing techniques for switching between both. Third, the tracking law is not necessarily bounded in angular velocity because Eq. (48) has an additional not-necessarily-bounded term. However, it has been seen in the simulations that the angular velocity remains bounded. This condition needs further study and could be addressed in the future. Fourth, this work deals only with static hard conic constraints. Extending the results to dynamic hard conic constraints, where the axis of the cone is not inertially fixed, might be possible.

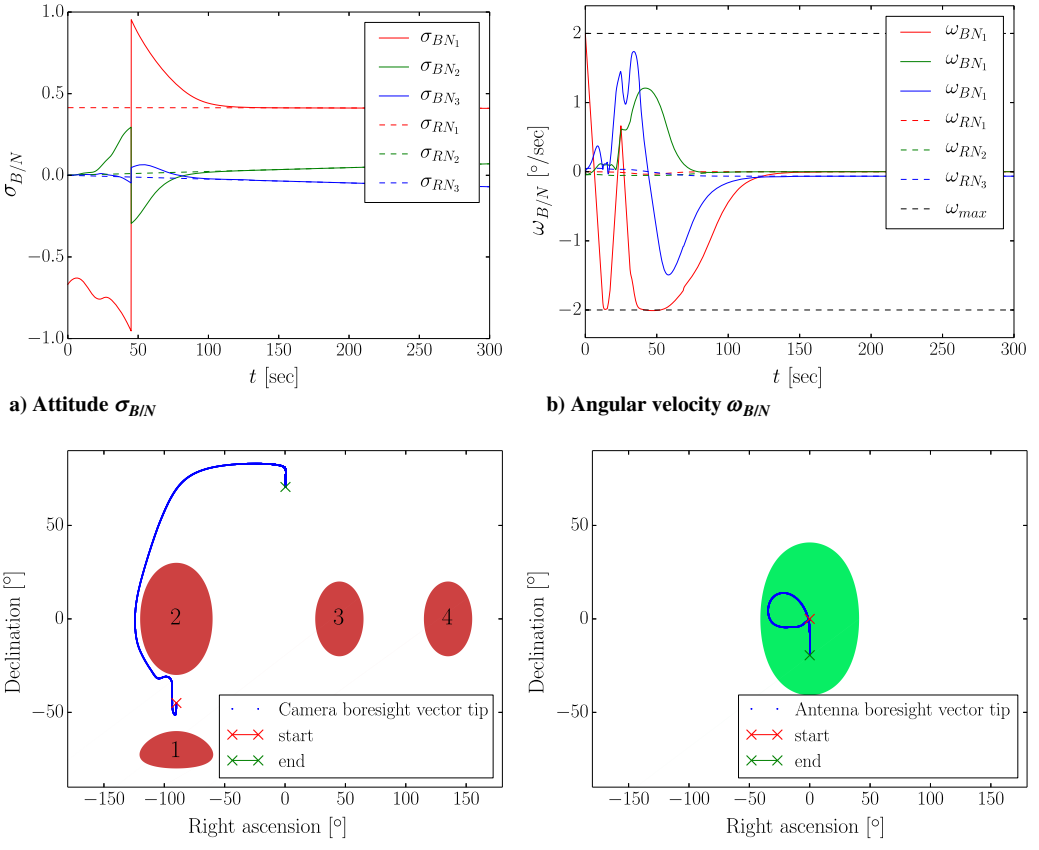

a) Attitude $\sigma_{B/N}$ **b) Angular velocity $\omega_{B/N}$**

c) Cylindrical projection of the exclusion zones **d) Cylindrical projection of the inclusion zones**

Fig. 6 Tracking control performance illustration.

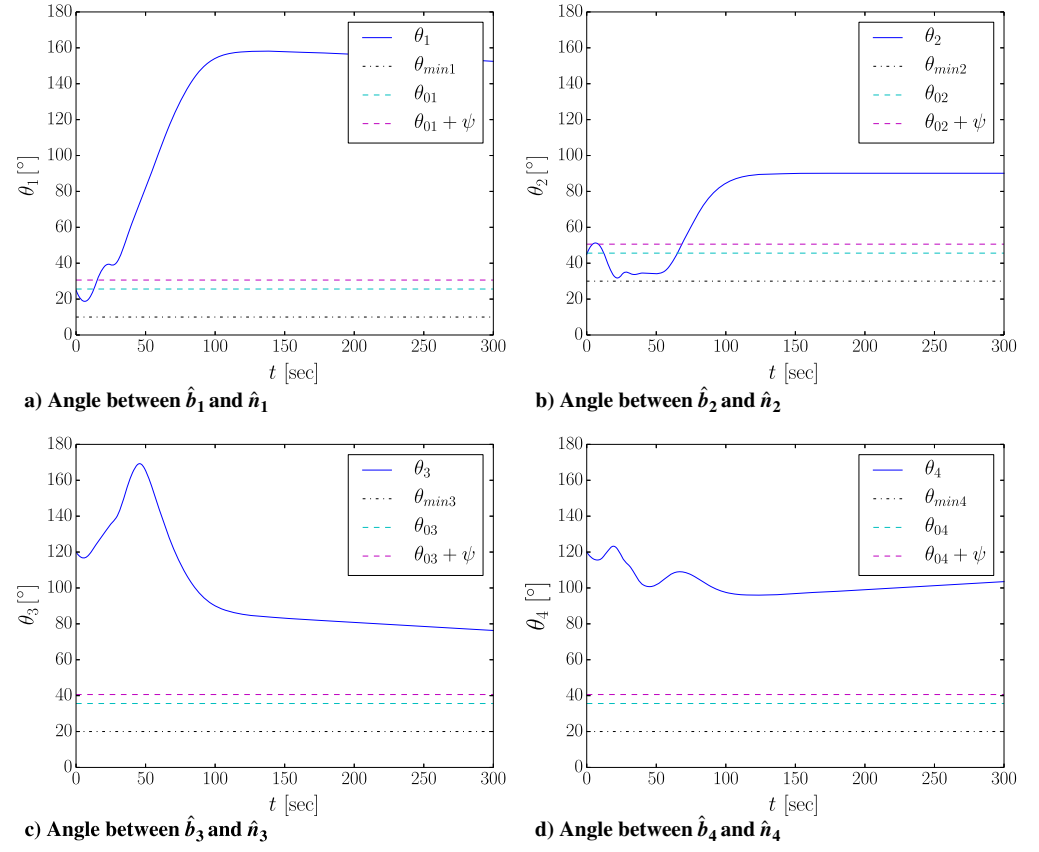

a) Angle between $\hat{b}_1$ and $\hat{n}_1$ **b) Angle between $\hat{b}_2$ and $\hat{n}_2$**

c) Angle between $\hat{b}_3$ and $\hat{n}_3$ **d) Angle between $\hat{b}_4$ and $\hat{n}_4$**

Fig. 7 Tracking control performance illustration. Exclusion constraint angles. Exclusion zones 3 and 4 are not considered by Algorithm 2 because they are "far" from the trajectory.

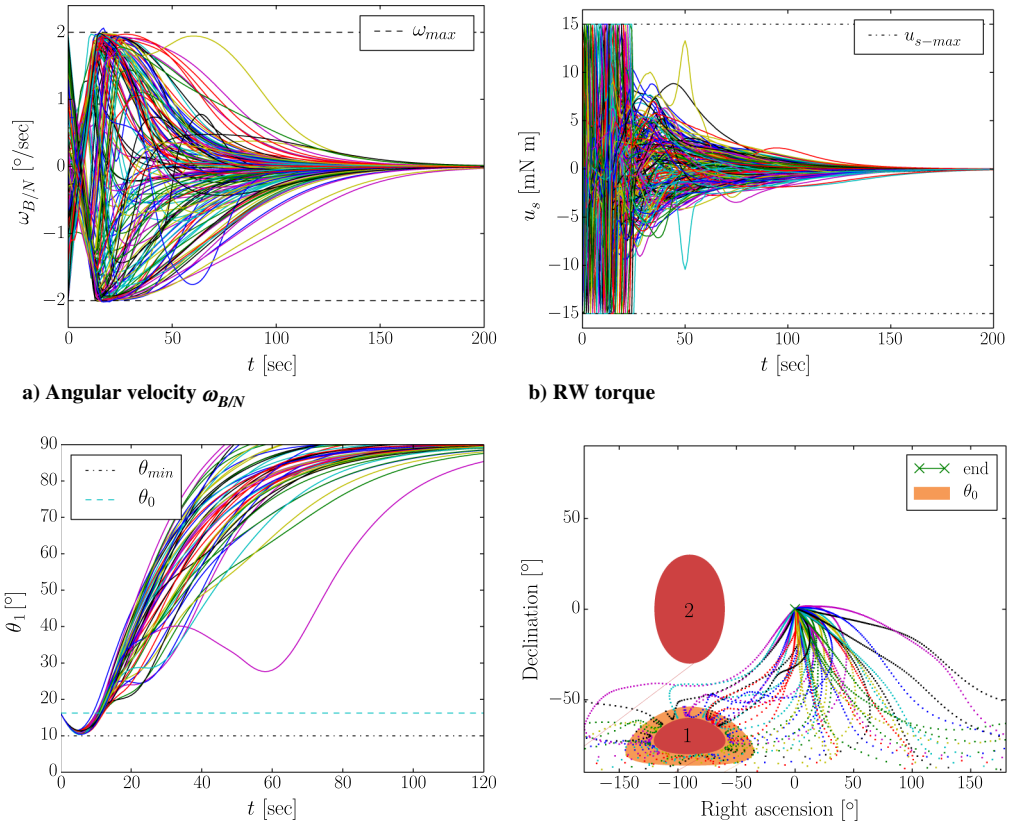

a) Angular velocity $\omega_{B/N}$ **b) RW torque**

c) Angle between $\hat{n}_1$ and $\hat{b}_1$ **d) Cylindrical projection map**

Fig. 8 Monte Carlo simulation.

Fifth, the repelling effect in the vicinity of a constraint given by α_i and β_i has not been addressed and might be studied in the future. In other words, these two sets of parameters can be used to change the repelling force in the vicinity of the cones.

XI. Conclusions

Orientation-constrained attitude control is not a mature technology. In fact, it is a lively active research topic with several different proposed solutions. The strength of Lyapunov-derived methods is that they have low complexity from an algorithmic point of view. Indeed, few closed-form function evaluations are usually required. Unfortunately, the current available Lyapunov-derived techniques do not limit angular rate and control torque, which makes them hardly applicable to real attitude constrained control problems. Furthermore, they do not solve the tracking problem either. This paper extends the benefits of using Lyapunov-derived methods to rate-and-torque-bounded problems. Furthermore, the tracking problem with orientation constraints is also solved.

Bounded angular velocity is achieved in the regulation problem using a kinematic steering law to control the attitude of a spacecraft with RWs under static hard conic constraints. The algorithm works well with any number of constraints, even in highly symmetric conditions. Bounded control torque can be achieved by extending the exclusion cones to take into account the limited control torque capacity of the spacecraft. The extended cones are not much larger than the original exclusion cones, being a function of the minimum torque capability of the RW array of the spacecraft. As a corollary, this result makes it possible, if desired, to switch from the constrained steering law to the unconstrained steering law when sufficiently far from the constraint cones.

References

[1] Kim, Y., Mesbahi, M., Singh, G., and Hadaegh, F., "On the Convex Parameterization of Spacecraft Orientation in Presence of Constraints and its Applications," *IEEE Transactions on Aerospace and Electronic Systems*, Vol. 46, No. 3, 2010, pp. 1097–1109. doi:10.1109/TAES.2010.5545176

[2] Hablani, H., "Attitude Commands Avoiding Bright Objects and Maintaining Communication with Ground Station," *Journal of Guidance, Control, and Dynamics*, Vol. 22, No. 6, 1999, pp. 759–767. doi:10.2514/2.4469

[3] Spindler, K., "New Methods in On-Board Attitude Control," *Advanced in the Astronautical Sciences*, Vol. 100, No. 2, 1998, pp. 111–124.

[4] Frakes, J. P., Henretty, D. A., Flatley, T. W., Markley, F. L., San, J., and Lightsey, E. G., "SAMPEX Science Pointing with Velocity Avoidance," *Proceedings of the AAS/AIAA Spaceflight Mechanics Meeting*, AAS Paper 92-182, San Diego, CA, 1992, pp. 949–966.

[5] Biggs, J. D., and Colley, L., "Geometric Attitude Motion Planning for Spacecraft with Pointing and Actuator Constraints," *Journal of Guidance, Control, and Dynamics*, Vol. 39, No. 7, 2016, pp. 1672–1677. doi:10.2514/1.G001514

[6] Singh, G., Macala, G., Wong, E., and Rasmussen, R., "A Constraint Monitor Algorithm for the Cassini Spacecraft," *Proceedings of the AIAA Guidance, Navigation, and Control Conference*, AIAA, Reston, VA, 1997, pp. 272–282. doi:10.2514/6.1997-3526

[7] Ahmed, A., Alexander, J., Boussalis, D., Breckenridge, W., Macala, G., Mesbahi, M., San Martin, M., Singh, G., and Wong, E., *Cassini Control Analysis Book*, Jet Propulsion Lab., California Inst. of Technology, Pasadena, CA, 1998.

[8] Kim, Y., Mesbahi, M., and Hadaegh, F., "Dual-Spacecraft Formation Flying in Deep Space: Optimal Collision-Free Reconfigurations," *Journal of Guidance, Control, and Dynamics*, Vol. 26, No. 2, 2003, pp. 375–379. doi:10.2514/2.5059

[9] Frazzoli, E., Dahleh, M., Feron, E., and Kornfeld, R. P., "A Randomized Attitude Slew Planning Algorithm for Autonomous Spacecraft," *Proceedings of the AIAA Guidance, Navigation, and Control Conference and Exhibit*, AIAA, Reston, VA, Aug. 2001. doi:10.2514/6.2001-4155

[10] Boyd, S., and Vandenberghe, L., *Convex Optimization*, 1st ed., Cambridge Univ. Press, 2004, Chap. 44.

[11] Kim, Y., and Mesbahi, M., "Quadratically Constrained Spacecraft Attitude Constrained Control via Semidefinite Programming," *IEEE*

Transactions on Automatic Control, Vol. 49, No. 5, 2004, pp. 731–735. doi:10.1109/TAC.2004.825959

[12] Sun, C., and Dai, R., "Spacecraft Attitude Control under Constrained Zones via Quadratically Constrained Quadratic Programming," *AIAA Guidance, Navigation, and Control Conference*, AIAA, Reston, VA, 2015. doi:10.2514/6.2015-2010

[13] Kjellberg, H., and Lightsey, G., "Discretized Constrained Attitude Pathfinding and Control for Satellites," *Journal of Guidance, Control, and Dynamics*, Vol. 36, No. 5, 2013, pp. 1301–1309. doi:10.2514/1.60189

[14] Tanygin, S., "Fast Three-Axis Constrained Attitude Pathfinding and Visualization Using Minimum Distortion Parameterizations," *Journal of Guidance, Control, and Dynamics*, Vol. 38, No. 12, 2015, pp. 2324–2336. doi:10.2514/1.G000974

[15] McInnes, C. R., "Large Angle Slew Maneuvers with Autonomous Sun Vector Avoidance," *Journal of Guidance, Control, and Dynamics*, Vol. 17, No. 4, 1994, pp. 875–877. doi:10.2514/3.21283

[16] Lee, U., and Mesbahi, M., "Spacecraft Reorientation in Presence of Attitude Constraints via Logarithmic Barrier Potentials," *Proceedings of the American Control Conference*, New York, 2011, pp. 450–455. doi:10.1109/ACC.2011.5991284

[17] Lee, U., and Mesbahi, M., "Feedback Control for Spacecraft Reorientation under Attitude Constraints via Convex Potentials," *IEEE Transactions on Aerospace and Electronic Systems*, Vol. 50, No. 4, 2014, pp. 2578–2592. doi:10.1109/TAES.2014.120240

[18] Wisniewski, R., and Kulczycki, P., "Slew Maneuver Control for Spacecraft Equipped with Star Camera and Reaction Wheels," *Control Engineering Practice*, Vol. 13, No. 3, 2005, pp. 349–356. doi:10.1016/j.conengprac.2003.12.006

[19] Marandi, S. R., and Modi, V. J., "A Preferred Coordinate System and the Associated Orientation Representation in Attitude Dynamics," *Acta Astronautica*, Vol. 15, No. 11, 1987, pp. 833–843. doi:10.1016/0094-5765(87)90038-5

[20] Lee, U., "State-Constrained Rotational and Translational Motion Control with Applications to Monolithic and Distributed Spacecraft," Ph.D. Dissertation, Univ. of Washington, Seattle, WA, 2014.

[21] Schaub, H., and Junkins, J. L., *Analytical Mechanics of Space Systems*, 3rd ed., AIAA Education Series, AIAA, Reston, VA, 2014, Chaps. 3 and 4.

[22] Schaub, H., and Piggott, S., "Speed-Constrained Three-Axes Attitude Control Using Kinematic Steering," *Acta Astronautica*, Vol. 147 June 2018, pp. 1–8. doi:10.1016/j.actaastro.2018.03.022

[23] Wiener, T. F., "Theoretical Analysis of Gimballess Inertial Reference Equipment Using Delta-Modulated Instruments," Ph.D. Dissertation, Dept. of Aeronautics and Astronautics, Massachusetts Inst. of Technology, Cambridge, MA, March 1962.

[24] Shuster, M. D., "A Survey of Attitude Representations," *Journal of the Astronautical Sciences*, Vol. 41, No. 4, 1993, pp. 439–517.

[25] Hurtado, J. E., "Interior Parameters, Exterior Parameters, and a Cayley-Like Transform," *Journal of Guidance, Control, and Dynamics*, Vol. 32, No. 2, 2009, pp. 653–657. doi:10.2514/1.39624

[26] Khalil, H., *Nonlinear Systems*, 3rd ed., Prentice Hall, 2002, Chaps. 4 and 14.

[27] Kim, K.-S., and Kim, Y., "Robust Backstepping Control for Slew Maneuver Using Nonlinear Tracking Control," *IEEE Transactions on Control Systems Technology*, Vol. 11, No. 6, 2003, pp. 822–829. doi:10.1109/TCST.2003.815608

[28] Press, W., Teukolsky, S., Vetterling, W., and Flannery, B., *Numerical Recipes: The Art of Scientific Computing*, 3rd ed., Cambridge Univ. Press, 2007, Chap. 5.

[29] Oppenheim, A., and Schafer, R., *Discrete-Time Signal Processing*, 2nd ed., Prentice Hall, 1998, Chap. 2.

[30] Tee, K., Ge, S., and Tay, E., "Barrier Lyapunov Functions for the Control of Output-Constrained Nonlinear Systems," *Automatica*, Vol. 45, No. 4, 2009, pp. 918–927. doi:10.1016/j.automatica.2008.11.017

[31] Landis Markley, F., Reynolds, R., Liu, F., and Lebsock, K., "Maximum Torque and Momentum Envelopes for Reaction-Wheel Arrays," *Journal of Guidance, Control, and Dynamics*, Vol. 33, No. 5, 2010, pp. 1606–1614. doi:10.2514/1.47235

[32] Schmitt, O. H., "A Thermionic Trigger," *Journal of Scientific Instruments*, Vol. 15, No. 1, 1938, pp. 24–26. doi:10.1088/0950-7671/15/1/305